HYDROGEOCHEMICAL EVOLUTION OF GROUNDWATERS IN THE WILLISTON BASIN, CANADA

A Thesis Submitted to the College

of Graduate and Postdoctoral Studies

In Partial Fulfillment of the Requirements

For the Degree of Master of Science

In the Department of Geological Sciences

University of Saskatchewan

Saskatoon

By

AIDAN CHRISTINA MOWAT

PERMISSION TO USE

In presenting this thesis in partial fulfillment of the requirements for a Postgraduate degree from the University of Saskatchewan, I agree that the Libraries of this University may make it freely available for inspection. I further agree that permission for copying of this thesis in any manner, in whole or in part, for scholarly purposes may be granted by the professor or professors who supervised my thesis work or, in their absence, by the Head of the Department or the Dean of the College in which my thesis work was done. It is understood that any copying or publication or use of this thesis or parts thereof for financial gain shall not be allowed without my written permission. It is also understood that due recognition shall be given to me and to the University of Saskatchewan in any scholarly use which may be made of any material in my thesis.

Requests for permission to copy or to make other uses of materials in this thesis/dissertation in whole or part should be addressed to:

Head of the Department of Geological Sciences
114 Science Place
University of Saskatchewan
Saskatoon, Saskatchewan S7N 5E2 Canada

Or

Dean
College of Graduate and Postdoctoral Studies
University of Saskatchewan
116 Thorvaldson Building, 110 Science Place
Saskatoon, Saskatchewan S7N 5C9 Canada

ABSTRACT

Glacial cycles over the last two million years have successfully altered deep groundwater flow in the Williston Basin, Canada. Mixing with evaporated paleoseawater has resulted in unique geochemical signatures in formation waters with spatial and temporal trends, however the timing of glaciogenic recharge into the Williston Basin and spatial understanding of the flow system is loosely constrained. I examine timing and effect of glaciogenic recharge by using an integration of fluid chemistry, stable isotope data, and transport modeling. Results demonstrate that meltwater arrived at depths of ~600 to 1000 m in the northcentral region of the Williston Basin at two separate time periods, 75 to 150 ka and 300 ka. Spatial analysis of geochemical data illustrates that meltwater recharge extended to a continuous recharge belt along the northern margin of the Williston Basin, greater than previously anticipated. Individual and multi-variate analysis of isotope and solute geochemistry exhibit trends that contribute to fractionation of $\delta^{18}O$, $\delta^{2}H$, $^{87}Sr/^{86}Sr$, $\delta^{37}Cl$, and $\delta^{81}Br$, and validates the importance of water origin and variation in mineral composition on solute concentrations and isotope values. Although overprinting and mixing interactions may present challenges in geochemical interpretation, the inter-disciplinary approach used in this research contributes to a greater understanding of how glacial meltwater recharge altered geochemical landscapes during large-scale salt dissolution in the Williston Basin.

ACKNOWLEDGEMENTS

I would like to thank all my friends and family for their continuous support and encouragement throughout my endeavors. I would like to thank Dr. Matthew Lindsay and Dr. Grant Ferguson for believing in me and taking me as an undergraduate and graduate student. Thank you both for the support−physical, emotional, and mental−you have given me over the 6 years of supervision.

I would like to thank all of the Environmental Geochemistry Research Group through my time at USask, including (but not limited to): Colton Vessey, Daniel Francis, Mattea Cowell, Sarah Rudderham, and Emily Champion. You have all been an amazing support group over the years. Besides my immediate research group, Matthew Nadeau, Courtney Onstad, Katelynn Brown, Katrina Dorosh, and Rebecca Bush are all friendships which I cherish over the years of undergraduate and graduate school.

I would like to thank the faculty and staff in the Department of Geological Science at the University of Saskatchewan for the project support, and the participating potash companies: Nutrien Ltd., BHP Billiton, and The Mosaic Company. In addition to Dr. Lindsay and Dr. Ferguson, thank you to Dr. Jennifer McIntosh for being a massive pillar of support and encouragement.

Lastly, I would like to thank my mother, Cheryl, my grandparents Ben and Dianne, my close friend, Katie, and my partner, Toby, for being my biggest cheerleaders, mentors, and best friends.

TABLE OF CONTENTS

LIST OF FIGURES

LIST OF TABLES

LIST OF ABBREVIATIONS

TDS	Total dissolved solids
‰	Per mille
VSMOW	Vienna Standard Mean Ocean Water
SMOC	Standard Mean Ocean Chloride
SMOB	Standard Mean Ocean bromide
SRM	Standard reference material
GMWL	Global Meteoric Water Line
LMWL	Local meteoric water line
HDPE	High Density Polyethylene
GC−CF−IRMS	Gas chromatography continuous flow isotope ratio mass spectrometry
PCA	Principal component analysis

CHAPTER 1: INTRODUCTION

Major geologic events must ensue for continental–scale groundwater flow systems to be altered. Glacial cycles over the last two million years were successful in greatly altering these flow systems by increasing hydraulic heads and recharging subglacial meltwaters to kilometre depths in permeable formations (Grasby et al., 2000; Person et al., 2007; McIntosh et al., 2012). From dilution to complete flushing of remnant paleoevaporated fluids, the hydrogeologic landscape of sedimentary basins was changed over the last two million years.

Glacial recharge has impacted sedimentary basins across the northern hemisphere as evidenced by using physical geography and geochemical observations (Boulton et al., 1996; Grasby et al., 2000) resulting in major changes to loading structures and instabilities in near-surface formations. In particular, in North America where glacial activity has occurred along mid-latitudes in the Western Canada Sedimentary Basin and Michigan/Illinois/Appalachian basins (Grasby et al., 2000; Person et al., 2007; McIntosh et al., 2012), massive regions of salt dissolution have resulted in vastly different geochemical signatures and major changes to energy and mineral resources.

The Williston Basin, located in the Western Canada Sedimentary Basin, is no exception to the effects of Pleistocene glaciation (Grasby et al., 2000; Person et al., 2007). However, timing of glaciogenic recharge responsible for flushing evaporated and dissolution of evaporites remain vaguely constrained. Previous studies highlight the importance of the eastern margin of the Williston Basin for these recharge events, but evidence suggests there is a similar amount of recharge occurring along the northern margin as well. Additionally, minimal research has been

done to construct how the hydrostratigraphy in regions across the Williston Basin vary together, or as separate entities, and how the geochemical variables evolve with glaciogenic flushing and mineral dissolution.

1.1 Research Hypothesis and Objectives

This thesis examines the timing and extent of glaciogenic recharge and relative effects on remnant saline fluids in deep, subsurface aquifers of the Williston Basin. This is observed by simulating meltwater recharge in the last two million years to the Williston Basin, and collecting mine solute and isotope geochemistry data to understand statistical and qualitative correlations between selected variables. Specifically, these objectives include:

- Objective 1: simulate 1–D vertical transport in Devonian carbonate aquifers to the Williston Basin to confirm the ages of glaciogenic-origin groundwater, and map the transport ages to estimate flow paths and recharge zones along the Williston Basin margin.
- Objective 2: use bivariate and multivariate analysis to understand the variation in geochemistry between glaciogenic and brine sources.

1.2 Thesis Organization

This manuscript-style thesis consists of one published research paper (Chapter 2), a second research chapter (Chapter 3), and summary of observations (Chapter 5). The first research paper (Chapter 2) analyzes the variability in timing and transport of Pleistocene meltwater recharge to regional aquifers in the Williston Basin. Following the study conducted in Chapter 2, questions arose regarding the ability of various geochemical and isotopic tracers to evolve with different sources of saline fluids (e.g. from salt dissolution or paleoevaporated seawater). Therefore, the second chapter (Chapter 3) explores the geochemical variation in

solutes and isotope systems between evaporated paleoseawater and glaciogenic sourced groundwaters in the Williston Basin. The results from Chapter 2 and 3 compliment each other in identifying trends in solute and isotope chemistry and the driving factors to geochemical changes in deep, subsurface aquifers of the Williston Basin.

CHAPTER 2: VARIABILITY IN TIMING AND TRANSPORT OF PLEISTOCENE MELTWATER RECHARGE TO REGIONAL AQUIFERS

Abstract

The impacts of Pleistocene glaciation on groundwater flow systems in sedimentary basins are widely recognized, but the timing and distribution of subglacial recharge events remain poorly constrained. We investigate the spatial and temporal variability of recharge events from glaciations over the last two million years in the Williston Basin, Canada. Integration of fluid chemistry, stable isotope data, and transport modeling indicate that meltwater arrived at depths of ~600 to 1000 m in the northcentral region of the Williston Basin at two separate time periods, 75 to 150 ka and 300 ka, which we attribute to permeability differences between stacked aquifer systems. Our findings indicate that meltwater recharge extended along the northern margin of the Williston Basin as well as previously identified recharge areas to the east. Given the distance of measurements from recharge areas, evidence of recharge from the early to mid-Pleistocene appears to be preserved in the Williston Basin.

2.1 Introduction

Pleistocene glaciation profoundly altered continental–scale groundwater flow systems by increasing hydraulic heads and recharging fresh subglacial meltwaters to kilometre depths in underlying sedimentary basins (Grasby et al., 2000; Person et al., 2007; McIntosh et al., 2012). Advance and retreat of ice sheets produced multiple subglacial recharge events, which flushed and diluted remnant saline fluids (McIntosh et al., 2012) and extensively dissolved evaporites (Grasby and Chen, 2005; McIntosh and Walter, 2006) in sedimentary basins of North America and Europe

(Boulton et al., 1994; Kloppmann et al., 2001). The few studies that have attempted to constrain the timing of subglacial recharge using age tracers (e.g., Mazor and Bosch, 1987; Schlegel et al., 2011) have been relatively coarse and focus on single aquifer or confined aquifer systems, while many of these sedimentary basins contain extensive stacked aquifers that were likely recharged intermittently over the past two million years.

Pleistocene glacial meltwaters are an important fresh groundwater resource in glaciated continental and coastal regions across the northern hemisphere (Grasby et al., 2000; Edmunds and Milne, 2001; Person et al., 2007; Person, 2007; McIntosh et al., 2011). Infiltration and recharge of meltwaters have implications for long-term radioactive waste and CO_2 storage (Lemieux et al., 2008; Lemieux et al., 2011), energy resources via stimulation of microbial methanogenesis in shales and coalbeds (Martini et al., 2008; McIntosh et al., 2012), and mineral resources via dissolution of potash deposits in the Williston Basin (Grasby et al., 2000). Thus, determining the timing and flowpaths of subglacial recharge is vital for assessing resource sustainability and understanding the paleohydrogeology of sedimentary basins.

Previous studies have used age tracers like radiocarbon (^{14}C), helium (^{4}He), and krypton (^{81}Kr) to constrain the timing of Pleistocene recharge (McIntosh and Walter, 2006; Cloutier et al., 2006; Schlegel et al., 2011; Hendry et al., 2013; Gerber et al., 2017). However, radiocarbon dating is limited to <~50,000 years and existing noble gas data is relatively sparse. As an alternative, stable isotopes of water ($\delta^{18}O$ and $\delta^{2}H$) data are more widely available (Ferguson and Jasechko, 2015; Jasechko, 2019), enabling higher-resolution studies. These data are also effective indicators of groundwater sources as modern meteoric waters, Pleistocene recharge, and evaporated paleoseawater typically exhibit distinct $\delta^{18}O$ and $\delta^{2}H$ signatures. Previous studies using numerical models estimated the arrival time of waters with distinct isotopic signatures (e.g., subglacial

meltwater recharge) at specified locations within the Williston Basin (Hendry et al., 2013; Hendry and Harrington, 2014). The numerical transport modeling solves for the time period(s) which has passed since the Pleistocene meltwater arrived in the region and, fitted to high-resolution $\delta^{18}O$ and $\delta^{2}H$ data, can effectively constrain the timing of subglacial meltwater arrival.

The impacts of Pleistocene glaciation on basinal-scale flow systems in the Williston Basin are widely recognized (Grasby et al., 2000; Person et al., 2007). However, the timing of meltwater recharge events responsible for flushing evaporated and dissolution of evaporites remain ambiguous. Evaporated paleoseawater, positioned deep within the Williston Basin, are highly saline (>350 g L^{-1} TDS) and have elevated $\delta^{18}O$ and $\delta^{2}H$ values characteristic of evaporated paleoseawater (Wittrup and Kyser, 1990). However, recharge of fresh Pleistocene meltwaters, with low $\delta^{18}O$ values, along the north to east margins of the Williston Basin flushed evaporated paleoseawater and generated new salinity via extensive salt dissolution (Wittrup and Kyser, 1990; Grasby et al., 2000; Grasby and Chen 2005; Tipton, 2018). Using 1–D transport modeling of $\delta^{18}O$−depth profiles, Hendry et al. (2013) estimated Pleistocene subglacial recharge for the Cretaceous Mannville aquifer in southeast Saskatchewan, Canada arrived between 240 and 430 ka. The variation in arrival times to the Mannville aquifer may be attributed to local and regional discontinuities between locations, the distance to different recharge areas, and (or) changes in hydraulic properties (e.g. hydraulic conductivity or porosity).

Here, we explore the timing of Pleistocene meltwater recharge into a deep, stacked carbonate aquifer system at different locations within the Williston Basin to gain a more basin-scale perspective using a combination of high-resolution $\delta^{18}O$ and $\delta^{2}H$ data with groundwater transport modeling. We show that arrival times varied incoherently with spatial location and aquifer position in the carbonates, but that it consistently occurred within two separate time periods and from areas

along a continuous recharge belt along the north to east margin of the basin. This contributes a greater understanding of glacial meltwater recharge and flowpaths in the Williston Basin, and also its relevant applicability to other sedimentary basins impacted by glaciation in the northern hemisphere.

2.2 Regional Hydrogeology

The Williston Basin is an intracratonic sedimentary basin centered in North Dakota, USA. The basin extends north into southcentral Saskatchewan and southwest Manitoba in Canada, and west and south into Montana and South Dakota, respectively, in the USA. The basin is structurally bound by the Sweetgrass Arch to the west, the Canadian Shield to the north, the Manitoba Escarpment to the east, and various uplifts in Montana and South Dakota to the south (Kent and Christopher, 1994) (Figure 2–1). The Williston Basin consists of sedimentary rocks conformably and unconformably overlain by each other. Middle and upper Devonian (mid-Paleozoic) strata are composed of stacked aquifers, aquitards, and aquicludes that were deposited during carbonate transgressive and regressive episodes. These strata include the Prairie Evaporite aquiclude, Manitoba aquifer, Souris River aquitard, Duperow aquifer, Seward aquitard, Birdbear aquifer, and Three Forks aquitard (Figure 2–1).

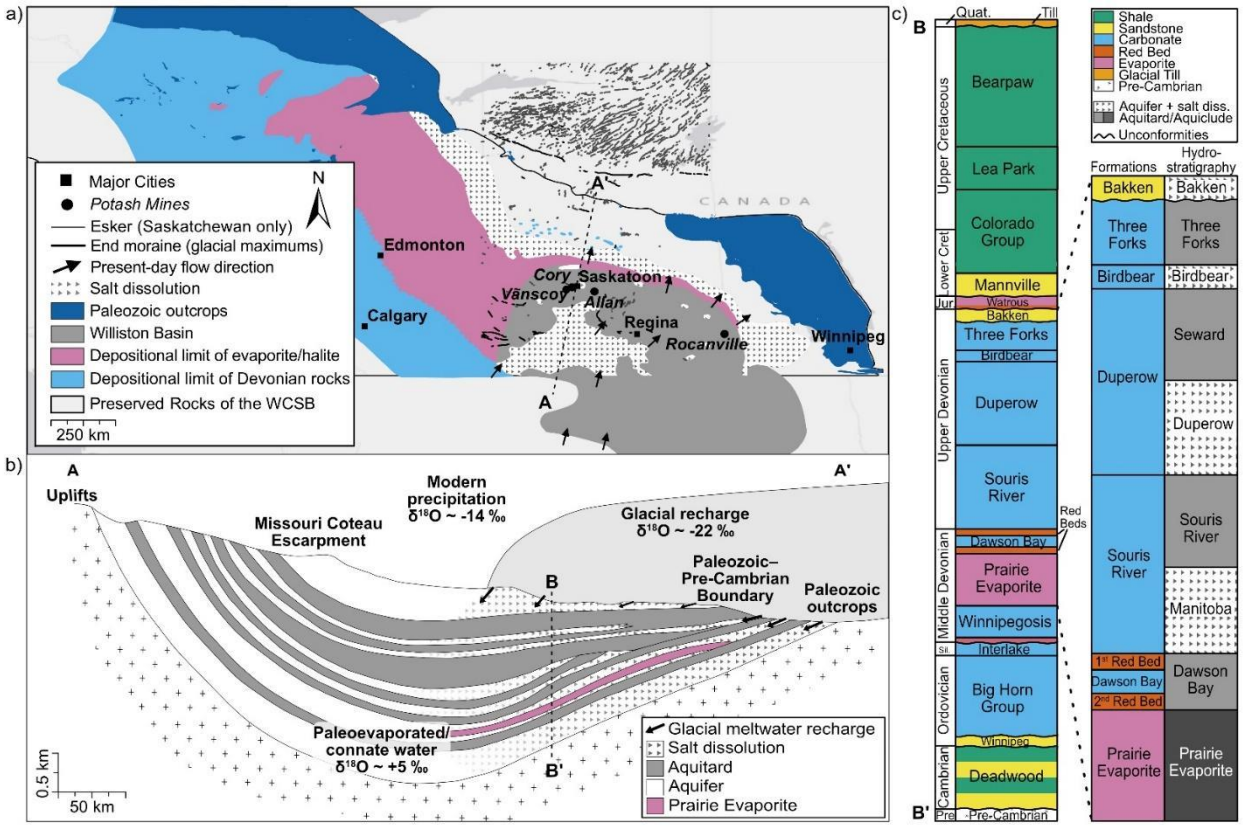

Figure 2–1: Overview of (a) Western Canada Sedimentary Basin and relevant geologic features with present−day regional flow directions, (b) cross section for the Williston Basin between A–A' with meltwater infiltration and mixing process during glacial impact, and (c) stratigraphic column of the Williston Basin between B–B' with the Devonian inset with more detailed geology and hydrostratigraphy surrounding the aquifers examined in this study.

The Williston Basin has been intermittently overlain by continental ice sheets over the past two million years (Christiansen and Sauer, 2001). Increases in the hydraulic head associated with ice sheets and subsequent influx of glacial meltwater into Paleozoic carbonate aquifers significantly altered groundwater flow patterns in the basin (Grasby et al., 2000). Groundwater within these carbonate aquifers, which are relatively isolated at-depth between adjacent confining units of shale and bedrock, retain a distinct geochemical and isotopic signature characteristic of Pleistocene meltwaters (Grasby and Betcher, 2002; Grasby and Chen, 2005). These characteristics include $\delta^{18}O$ and $\delta^{2}H$ values that plot on the Global Meteoric Water Line (GMWL) but more ^{18}O

and ^{2}H–depleted with respect to modern precipitation. They also exhibit a molar Na:Cl ratio of ~1 and Cl:Br ratios ~10 times greater than seawater, indicative of halite and salt dissolution (Grasby and Betcher, 2000)

Following retreat of the Laurentide Ice Sheet, hydraulic heads in the Williston Basin likely returned to the present, quasi-equilibrium state (Hitchon, 1969a; Grasby and Chen, 2005). Present−day regional groundwater flow is from topographic highs in the southwest, including the Black Hills in South Dakota, to topographic lows near the boundary of the Canadian Shield in the northeast (Figure 2–1a). The deepest hydrostratigraphic units of the Williston Basin exhibit little evidence of meteoric water circulation (Palombi, 2008). Instead, these Na-Cl to Na-Ca-Cl type waters exhibit characteristics of evaporated paleoseawater including molar Na:Cl ratios < 0.85, Cl:Br ratios comparable to evaporated seawater, and $\delta^{18}O$ and $\delta^{2}H$ values that plot below the GMWL (Grasby and Betcher, 2002; Grasby and Chen, 2005; Ferguson et al., 2007; Tipton, 2018). Stagnation of evaporated paleoseawater within deep sedimentary basins is attributed to negative buoyancy associated with high TDS waters (Bachu and Hitchon, 1996; Palombi, 2008; Ferguson et al., 2018).

2.3 Methods

2.3.1 Sample collection and analysis

Formation fluids were collected in November 2016 and March 2018 from active seeps over short time intervals in mine shafts and mine workings at the Vanscoy, Cory, Allan, and Rocanville potash mines in southcentral Saskatchewan (Figure 2–1). These seeps primarily originated from the middle to upper Devonian strata from the Birdbear formation (~600 m) to the Prairie formation (~1100 m), which corresponds to mine level (Table A1). Fluids were collected into clean 250 mL or 1000 mL HDPE bottles and stored at ambient room temperature until analysis.

Dissolved Cl− and Br− concentrations were determined by ion chromatography in the Environmental Analytical Laboratory at the Saskatchewan Research Council (Saskatoon, Canada). The $\delta^{18}O$ and $\delta^{2}H$ values were determined using CO_2–H_2O and H_2–H_2O equilibration methods, respectively, at the Saskatchewan Isotope Laboratory (Saskatoon, Canada) and results are reported as the relative difference between the $^{18}O/^{16}O$ and $^{2}H/^{1}H$ abundance ratios normalized to Vienna Standard Mean Ocean Water (VSMOW), expressed in per mille (‰) notation. Accuracies of $\delta^{2}H$ and $\delta^{18}O$ are 2‰ and 0.2‰, respectively, but this methodology does not account for the salt effect in highly saline waters (Sofer and Gat, 1972; Sofer and Gat, 1975; Koehler et al., 2013). Corrections for the salt effect, which produces discrepancies in measured isotope compositions in high activity brines as outlined by Sofer and Gat (1972; 1975) and Koehler et al. (2013), were applied to the $\delta^{18}O$ and $\delta^{2}H$ values. Additional data (Cl, Br, $\delta^{18}O$, and $\delta^{2}H$) is from Tipton (2018) to increase data coverage.

2.3.2 Model setup

A simplified hydrostratigraphic column (Figure 2–2a) was constructed based on local geology using GeoHub Saskatchewan (Marsh and Love, 2014) for Prairie Evaporite (mine level) to surface. Simulation of measured $\delta^{18}O$ data follows a similar procedure as detailed by Hendry et al. (2013) to develop a diffusion model using the finite element model software CTRAN/W and SEEP/W (GeoStudio 2018 R2, v. 9.1.1.16749). In this approach, we simulate 1–D vertical transport from Devonian carbonate aquifers into adjacent aquitards by assigning a step change in aquifer groundwater concentration when meltwater first arrives in the study site via regional groundwater flow (Figure 2–2a-b). These models, which used a spacing between nodes of 10 m, assumes that prior to the arrival of meltwater, the vertical distribution of $\delta^{18}O$ was controlled by diffusion over tens of millions of years due to presence of relatively low regional groundwater

flow rates. Therefore, the arrival time of glacial meltwater recharge to the study region before present day, t = 0 ka, is the simulation period length which best fits observed data (t > 0 ka).

Solute transport is calculated based on:

(1) $\frac{\partial C}{\partial t} = D_e \frac{\partial^2 C}{\partial z^2} - v \frac{\partial C}{\partial z}$

(2) $v = \frac{q}{n_e}$,

where C is concentration, t is time, D_e is the effective diffusion coefficient, z is vertical distance, v is average linear velocity, q is specific discharge, and n_e is effective porosity.

We used n_e values reported by Hendry et al. (2013) based on laboratory measurements for the Quaternary glacial till (0.24), Cretaceous shales (0.33), lower Cretaceous sandstones (0.34), Devonian carbonates (0.10), and the Prairie Evaporite (0.33) based on measurements on core from a commercial database (IHS Energy, 2017). We used D_e values of 2.3 x 10^{-10} m^2 s^{-1} for glacial till, shale and sandstone units (Hendry and Wassenar, 1999), 1.32 x 10^{-10} m^2 s^{-1} for the Devonian carbonate aquifers, and 6.0 x 10^{-11} m^2 s^{-1} for the Prairie Evaporite (Boudreau, 1996; Boudreau and Meysman, 2006; Hendry et al., 2009). We increased D_e to 9 x 10^{-10} m^2 s^{-1} for the Devonian carbonate aquifers in the diffusion model set-up (Figure 2–2c).

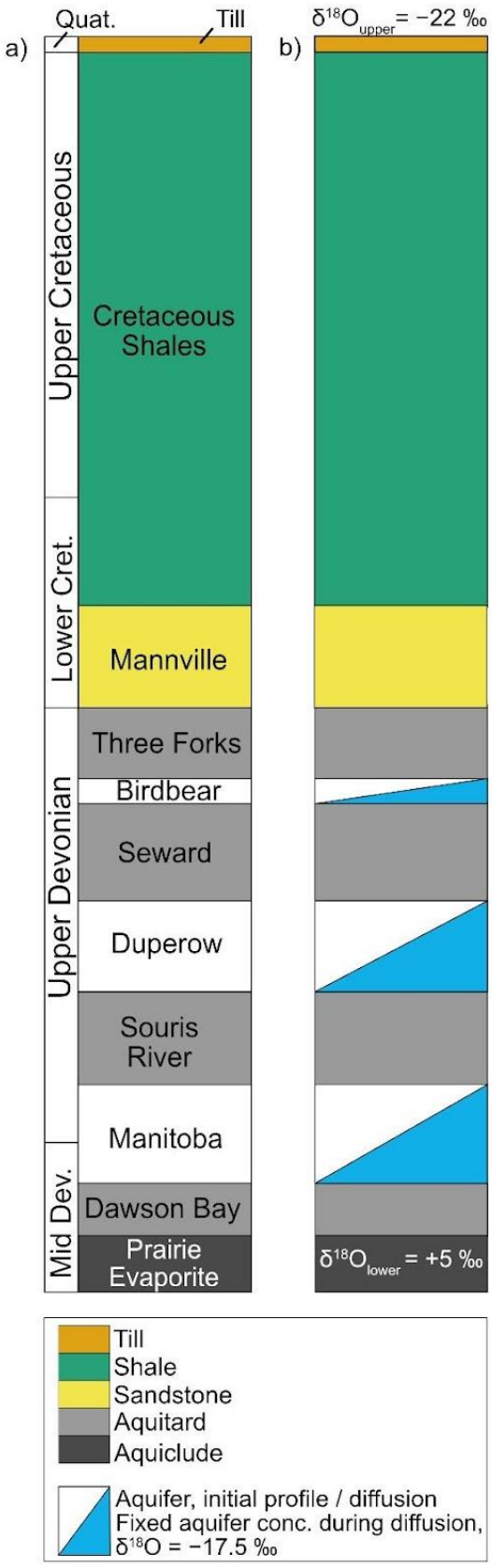

Figure 2–2: Conceptual build of 1-dimensional finite element model software in CTRAN/W and SEEP/W (GeoStudio 2018 R2, v. 9.1.1.16749). (a) initial profile with only upper and lower boundary conditions, and (b) diffusion-only profile set-up with upper and lower boundary conditions and constant concentration at each carbonate aquifer.

The initial hydrogeochemical profile, representing pre-glaciation conditions and (or) zero recharge, is simulated based on a diffusion-only transport setting (i.e., $v = 0$) after Hendry et al. (2013) between two fixed boundaries (Figure 2–2). Zero pressure was assigned to the top of the hydrostratigraphic column, and a bottom pressure head was assigned to the bottom of the column equivalent to the depth of the Prairie Evaporite formation (i.e. hydrostatic conditions): (Cory) 1025 m, (Vanscoy) 1025 m, (Allan) 1000 m, and (Rocanville) 950 m. The $\delta^{18}O$ values used for the constant concentrations of the upper and lower boundaries correspond to minimum and maximum isotope compositions recorded in the Western Canada Sedimentary Basin. We defined the upper boundary, $\delta^{18}O_{upper}$, for surface recharge −22‰ to reflect subglacial meltwater (Grasby and Chen,

2005; Ferguson et al., 2007; Ferguson and Jasechko, 2015) and the lower fixed boundary, $\delta^{18}O_{lower}$ at the Prairie Evaporite as +5‰ to represent evaporated paleoseawater (Grasby and Chen, 2005; Ferguson et al., 2007) (Figure 2−2a). The model simulated diffusive distribution from the upper to lower boundary for t = 100 million years until it reached steady state. However, the simulation matched unperturbed $\delta^{18}O$ data at t = 25 million years, and we used this profile as the initial concentration input for subsequent simulations (Figure S1). Next, we simulated vertical distribution between the aquifers and aquitards following arrival of subglacial meltwater recharge at the study sites. We performed a transient solute transport simulation of vertical diffusive transport (Figure 2–2b) over one million years from t_{intial} to t_{final}. This range covers the time period examined by Hendry et al. (2013) in their study of a shallower regional aquifer in our study area and encompasses much of the time where continental ice sheets covered this area of North America during the Pleistocene Epoch (Ehlers et al., 2008). In this scenario, we maintained the $\delta^{18}O_{upper}$ and $\delta^{18}O_{lower}$ values that defined the upper and lower boundary conditions, and defined the fixed aquifer concentrations, $\delta^{18}O_{aquifer}$, as −17.5‰ to reflect an average $\delta^{18}O_{aquifer}$ value for our dataset. Lastly, we increased D_e to 9 x 10^{-10} m^2 s^{-1} for the Devonian carbonate aquifers to reflect the effect of increased flow and mixing during a large recharge event. The best fit of meltwater arrival time(s) for each location were decided based on the qualitative and quantitative results between measured and simulated $\delta^{18}O$−depth profiles using root mean squared error (RMSE).

2.4 Results

2.4.1 Geochemical Results

The $\delta^{18}O$ values tended to be lower within aquifer units than in aquitards (Figure 2–3; Table A1), with these lower values generally falling on the GMWL (Figure 2–4a). $\delta^{2}H$ and $\delta^{18}O$ values fell along a mixing trend between the GMWL at a value consistent with a Pleistocene signature

(Ferguson and Jasechko, 2015) and a brine endmember resembling evaporated seawater (Figure 2–4a). Samples plotting near the GMWL tended to have high molar Cl:Br, while values below the GMWL had low molar Cl:Br (Figure 2–4b).

2.4.2 Model Results

The initial profile, describing the pre-glaciation conditions and (or) zero recharge, shows the best-fit to unperturbed $\delta^{18}O$ values at 25 million years and deviates greatly from the measured data after 40 million years (Figure S1). The upper and lower $\delta^{18}O$ boundary conditions (−22‰ and +5‰, respectively) provide a reasonable approximation of the estimated and known $\delta^{18}O$ values for glacial recharge (Grasby and Chen, 2005; Ferguson et al., 2007; Ferguson and Jasechko, 2015) and evaporated paleoseawater (Grasby and Chen, 2005; Ferguson et al., 2007). It is evident from the initial depth profile (Figure 2–3) that additional transport processes must be imparted on this stacked aquifer system to closely replicate the observed present-day ^{18}O values by simulating a diffusion−dominated environment with perturbation by a ^{18}O-depleted source into carbonate aquifers in the last million years. These results indicate that meltwater arrived non-uniformly into Devonian stacked aquifers (deepest Manitoba, middle Duperow, and uppermost Birdbear) at given locations in the Williston Basin (Figure 2–3b-d). In each simulation, the model demonstrates the aquitard(s) response to meltwater that was transported from the aquitards ($\delta^{18}O_{aquifer}$ = 17.5‰) as *t* increases, and eventually creating a best-fit to observed data.

Our diffusion models provide the following arrival times to our study locations: (Cory) 150 ka and 300 ka, (Vanscoy) 75 ka, (Allan) 300 ka, and (Rocanville) 100 ka (Figure 2–3). There was no detectable shift in $\delta^{18}O$ values reflective of glacial meltwaters in the Duperow aquifer at Rocanville.

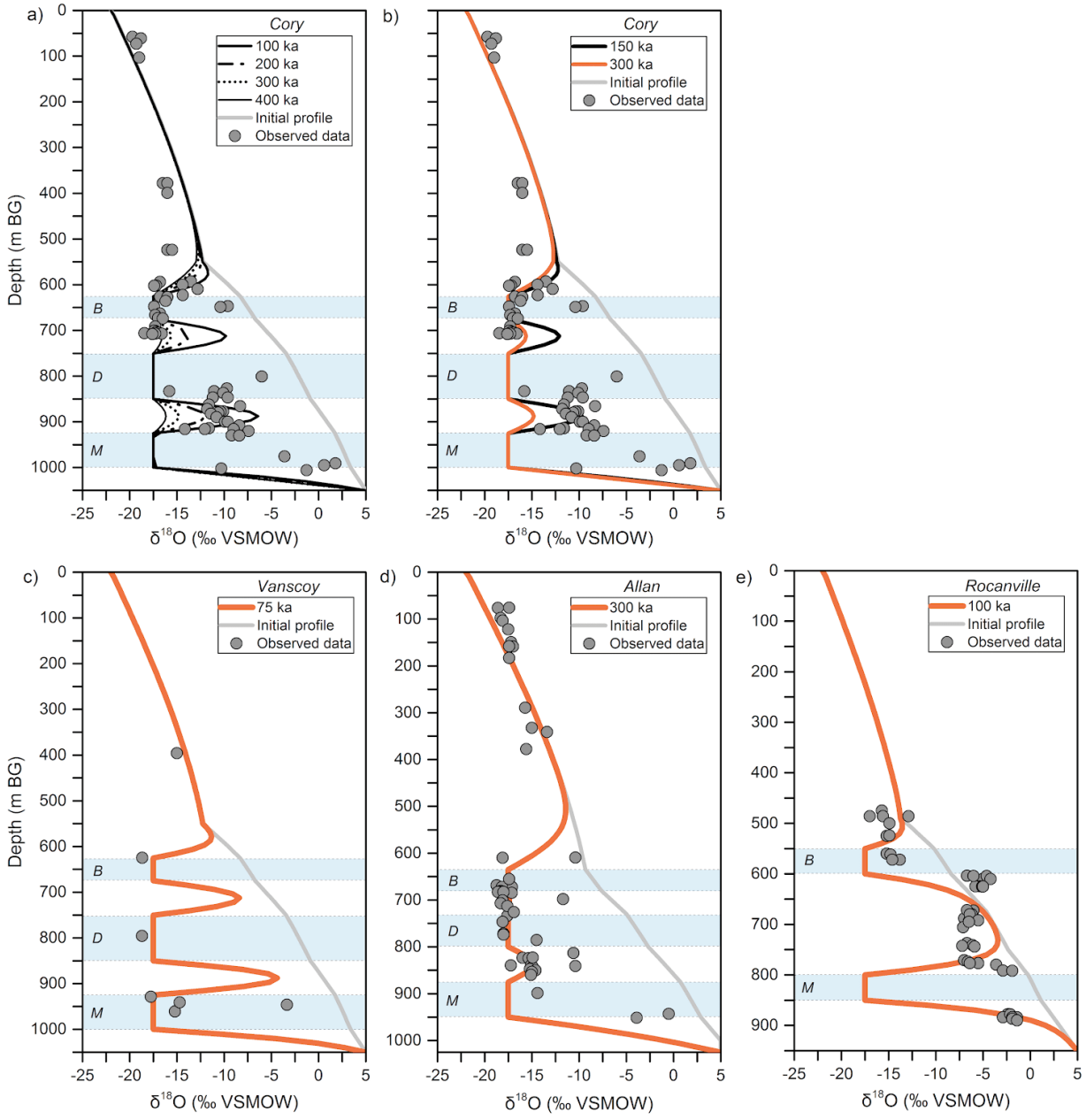

Figure 2–3: $\delta^{18}O$–depth profile results for (a) simulation of diffusion into aquitards between 100 ka and 400 ka at Cory with the initial profile included (light grey), and final best-fits of observed data for (b) Cory, (c) Vanscoy, (d) Allan, and (e) Rocanville. B = Birdbear, D = Duperow, and M = Manitoba aquifers.

These results, displaying perturbation of a freshwater source in carbonate aquifers, are complemented by $\delta^{18}O$ and $\delta^{2}H$ values that fall along the GMWL (Figure 4a) and higher Cl:Br

values, which indicate halite and salt dissolution (Figure 2–4b). In contrast, formation waters in the carbonate aquitards plot to the right of the GMWL (Figure 2–4a) and have relatively low Cl:Br values (< 2000; less than seawater) (Figure 2–4b). These brines derived from evaporation of paleoseawater (i.e., brine endmember in Figure 2–4a) which have been diluted by Pleistocene meltwaters, as indicated by the linear mixing trend in Figure 2–4a.

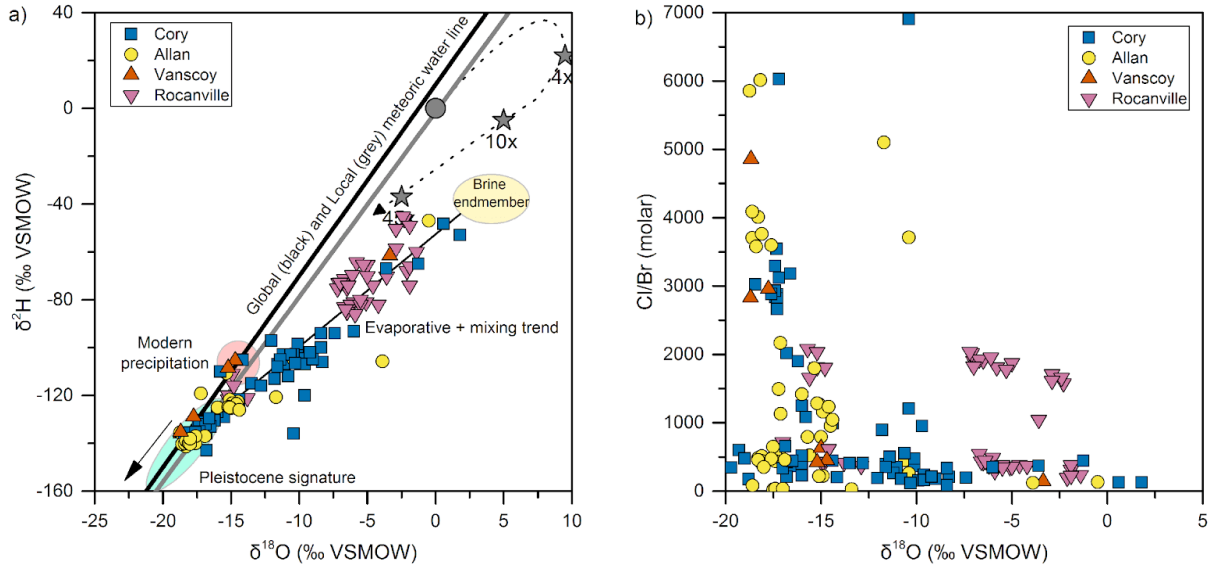

Figure 2–4: (a) $\delta^{18}O$ versus $\delta^{2}H$ values of formation waters from stacked carbonate aquifers from the four study sites relative to with the global (black) and local (grey) meteoric water lines, general evaporation sequence of seawater (grey circle and stars with amount of evaporation) to form brines, and endmember ranges for the Williston Basin evaporated paleoseawater, present-day meteoric water, and Pleistocene glacial meltwater. (b) $\delta^{18}O$ versus molar Cl:Br molar ratios.

2.5 Discussion

The distribution of $\delta^{2}H$ and $\delta^{18}O$ values and molar Cl:Br found at depth in Devonian carbonate aquifers in this study are consistent with other studies that have found preserved Pleistocene age groundwaters in the Williston Basin (Grasby et al., 2000; Ferguson et al., 2007; Hendry et al., 2013; Ferguson and Jasechko, 2015). The lowest $\delta^{18}O$ values are higher than the lowest values documented in the region (less than −24‰; Ferguson and Jasechko, 2015), (Figure

2–4) which likely reflects variability in the isotopic composition of ice sheets both spatially and temporally during the Pleistocene. However, the Pleistocene endmember (−17.5‰) is similar to other studies examining mixing between older brines and subglacial recharge (Grasby et al., 2000; Hendry et al., 2013) and is represented by a large portion of our data (Figure 2–4). The lowest δ^2H and $\delta^{18}O$ values are present in the Duperow, Manitoba and Birdbear aquifers at Cory, Vanscoy and Allan (Figure 2–3), while the aquitards at those sites have higher δ^2H and $\delta^{18}O$ values, indicating that the aquitards have retained some component of older, paleoevaporated seawater. At Rocanville, Pleistocene waters appear to have only arrived in the Birdbear and Manitoba aquifers, but not in the Duperow aquifer. The variability between stratigraphic positions and geographic locations is likely a function of local heterogeneity in geology and hydraulic properties.

The arrival times of subglacial meltwater to our study locations varied in two groups – a younger 75 ka to 150 ka and an older 300 ka (Figure 2–3). The arrival times are consistent with Pleistocene recharge as previously established by others (Grasby et al., 2000; Person et al., 2007; McIntosh et al., 2012). These provide minimum estimates of groundwater ages for these waters and does not account for time required for transport from their recharge areas, which are likely a few hundred kilometers to the north and northeast. If we account for the transport time from the recharge areas to our study regions, we expect groundwater recharge events to likely correspond to glacial events that occurred in the early to mid-Pleistocene (Person et al, 2007). Subglacial recharge with similar ages is likely preserved in other sedimentary basins that experienced multiple advances of Pleistocene continental ice sheets. Groundwater flowpaths in the Williston Basin and previously glaciated regions across the northern hemisphere would have varied substantially during these multiple advances due to changes in glacial thicknesses, temperatures of basal ice, and evolving hydrostratigraphy, making reconstruction of past hydrogeologic conditions difficult.

Modelled arrival times do not reveal a coherent relationship by geographic location, but – except for Cory – the times are similar between stratigraphic positions. Local variations in hydraulic properties, such as those associated with dissolution features in the Willison Basin (Christiansen et al., 1982; Christiansen and Sauer, 2001; Grasby et al., 2000; Tipton, 2018), likely resulted in the preferential movement of subglacial recharge in our study region and within the Williston Basin. These variations are also consistent with previous studies that have demonstrated the role of ice sheets in creating transient and complex flow patterns in sedimentary basins by effectively reorganizing groundwater flow over the past two million years (Person, 2007; Bense and Person, 2008). For example, groundwaters at depth in the Illinois Basin show a mixing zone between evaporated paleoseawater and Pleistocene meltwater dating up to 1.2 Ma (Siegel, 1991; McIntosh et al., 2002; McIntosh and Walter, 2006), while other aquifers in the Illinois Basin and Michigan Basin record groundwater ages greater than 50 ka (McIntosh and Walter, 2006). Additionally, previous studies provide evidence for emplacement of high volumes of Pleistocene-sourced groundwaters in deep aquifers of the Williston Basin between 135 ka and 430 ka (Hendry, 2013; Schmeling, 2014).

The extent of transport of meltwater recharge into the Williston Basin was previously approximated to be 300 km from major outcrop zones to the east and northeast in Manitoba (Grasby et al., 2000). Rocanville has been affected by meltwater influx more recently than study locations that are westward, demonstrating a lack of an east–west trend in the flowpaths. The lack of an east–west trend in our modelled arrival times suggests that recharge arriving at Cory, Vanscoy, and Allan likely occurred from the north near the Paleozoic−Precambrian boundary of the basin. In Rocanville, low molar Cl:Br values (< 2000 molar Cl:Br), which are associated with a paleoevaporated source, and ^{18}O-enriched groundwater (Figure 2–4) is opposite to the expected

trend if meltwater recharged solely from the east and was transported west–southwest. Instead, the observed salt dissolution across the northern edge of the Williston Basin (Marsh and Love, 2014) along with higher molar Cl:Br values, which result from addition of Cl by dissolution of halite, and ^{18}O−depleted groundwater at Cory, Vanscoy, and Allan (Figure 2–4) suggests a continuous recharge belt along the northern margin of the Williston Basin from Saskatchewan into Manitoba (Figure 2–1a). This finding is consistent with observations of widespread salt dissolution and mixing zones between evaporated paleoseawater and meltwater recharge in the northcentral region of the basin (Grasby and Chen, 2005; Tipton, 2018; Woroniuk et al., 2018). Esker distribution in northern Saskatchewan supports this hypothesis by demonstrating a sharp change in permeability at the boundary of Precambrian and sedimentary rocks (Figure 2–1; Grasby and Chen, 2005) where high-permeability sedimentary rocks will facilitate enhanced recharge. Anomalous TDS concentrations and Na:Cl ratios (Tipton, 2018) bolster interpretations of regionally variable flow paths across the Williston Basin and further illustrates the complexity in stacked carbonate sequences and subglacial recharge over several million years.

2.6 Conclusion

A combination of high-resolution stable isotope data, $\delta^{18}O$ and $\delta^{2}H$, with groundwater transport modeling provided a useful dating approach to resolve ambiguity concerning timing of emplacement of Pleistocene waters at depth into the Williston Basin. This technique allows us to present a constrained range of groundwater arrival times and an updated view of flowpaths and paleohydrogeology of the basin. Here, we demonstrate that the arrival times of glacial meltwater to our study regions were variable – between 75 ka to 150 ka and 300 ka – which emphasizes the complexity of this aquifer system. The simulations produce best-fits for the same arrival times at each individual study site, but we did not identify coherent trends between the geographic locations

as a whole. Our results support previously identified recharge from the east in Manitoba, but we also determine the likelihood of recharge from the north to form a continuous recharge belt along the entire north-to-east margin of the Williston Basin.

The arrival times found in this study provide a constraint on the timing of subglacial recharge. Given the distance of the measurements from where Paleozoic carbonates subcrop (Figure 2–1), subglacial recharge from the early to mid-Pleistocene appear to be preserved in the Williston Basin. However, the exact recharge locations and groundwater flow patterns are unknown and likely varied throughout the Pleistocene Epoch. Subglacial recharge of similar ages is likely preserved in many glaciated areas of the northern hemisphere. Multiple glacial advances would have affected groundwater flow patterns in the Williston Basin and other similar environments. Application of the approach used here, along with improving our understanding of glacial advances and noble gas sampling, may provide insights into how other environments evolved during the Pleistocene and shifted to present-day conditions.

2.7 Acknowledgments and Data

Funding was provided to G. Ferguson by Global Water Futures and the University of Saskatchewan Centennial Engagement Chair. Additional support is awarded to A. Mowat from the Natural Sciences and Engineering Research Council of Canada (NSERC) Canadian Graduate Scholarship – Master's Program (NSERC CGS-M), the NSERC Postgraduate Scholarship – Doctoral (NSERC PGS-D) Program, the University of Saskatchewan Dean's Scholarship, and the Saskatchewan Queen Elizabeth II Centennial Aboriginal Scholarship. We are grateful to Dr. S. L. Barbour for assistance in transport modeling and to K. Tipton for consultation about additional data. We also acknowledge two anonymous reviewers who provided constructive feedback that improved this research.

All data included in this manuscript are included in Tipton (2018), Table A1, and (or) at the following DOI: 10.5281/zenodo.5363453.

CHAPTER 3: GEOCHEMICAL EVOLUTION OF BRINES IN THE WILLISTON BASIN, CANADA

Abstract

Mixing between multiple fluid sources has led to distinct geochemical signatures in solute and isotope geochemistry of formation waters at depth in the Williston Basin, Canada. Observations of spatial and temporal trends in isotope and solute data identify three groups of formation waters at four different locations that can be explained by mixing between glaciogenic meteoric waters and paleoevaporated seawater. Results from this study help constrain groundwater flow paths and extent of glaciogenic perturbation (i.e., dilution/flushing of remnant saline fluids) between the four study sites. The results suggest that glaciogenic perturbance is greater from the northern margin versus from the eastern margin, migrating towards the center of the Willison Basin. Additionally, results demonstrate that Devonian carbonates formation waters at Allan and Cory have been the most impacted by meteoric flushing events, while Rocanville has been the least impacted by the most recent glaciogenic perturbance.

3.1 Introduction

The geochemistry of fresh glaciogenic waters contrasts greatly against paleoevaporated seawater-derived groundwaters (Grasby et al., 2000; McIntosh et al., 2012; Birks et al., 2019). Past studies on formation water geochemistry in the Williston Basin have largely focused on "fingerprinting" fluids from specific stratigraphic units but lack synthesis of the available geochemical data and how the geochemical systems are related or evolve during new mineral interactions or large-scale salt dissolution. Previous studies have reported data for sedimentary

basins that contributes to the overall knowledge of the hydrogeochemistry of sedimentary basins − mostly, these studies have used solute composition like Na, Cl, and Br, and stable isotopes of water (Rostron and Holmden, 2000; Jensen et al., 2006; Tipton, 2018). There have been a few studies to-date that have utilized novel solute isotope tracers to distinguish the sources of salinity and fluid-rock reactions (Marza et al., 2022; Eggenkamp et al., 1995; Shouakar-Stash, 2008), but the data is sparse. Thus, pairing these solute isotope tracers with higher-density solute composition data enhances our knowledge of how these groundwater flow systems are affected by large-scale salt dissolution and mixing of geochemically distinct water sources related to glaciogenic influx.

This study synthesizes new results of solute and isotope geochemistry in deep groundwater of the Williston Basin at several different locations (Cory, Vanscoy, Allan, and Rocanville potash mines) to understand the effect of extensive salt dissolution on the geochemical systems and improve our understanding of flow paths and fluid evolution in the Williston Basin. This research demonstrates local and regional variation in solute and isotope geochemistry and shows mixing of glacial meltwater and remnant paleoevaporated seawater, and salt dissolution. Although overprinting of basinal fluid signatures by glacial recharge in the last two million years may present challenges, this study combines multiple geochemical and isotopic tools to contribute to a greater understanding of the hydrologic landscape of the Williston Basin.

3.2 Regional geology

Details on the hydrogeology of the Williston Basin is outlined extensively in chapter 2, Figure 2−1. Briefly, the Williston Basin is a sedimentary basin centered in North Dakota, USA. Deep stacked aquifers, aquitards, and aquicludes are relatively isolated from the surface, which retains unique geochemical and isotopic signatures in the groundwater that allows us to discern

major geologic events. In this chapter, the lithology of the Williston Basin is important in understanding mineral dissolution and water-rock interactions during glacial meltwater recharge.

The Williston Basin is made up of sedimentary rocks: carbonates, evaporites, sandstones, and shales (figure 2−1). Evaporite deposits are interlayered within the carbonate sequences during deposition of these sediments. The main evaporite minerals present are sylvite (KCl) and halite (NaCl), with small amounts of carnallite ($KMgCl_3 \cdot 6(H_2O)$), anhydrite ($CaSO_4$) and gypsum ($CaSO_4 \cdot 2H_2O$); minor evaporite layers may be interbedded in units above the Prairie Evaporite consisting mostly of anhydrite (Holter, 1969). Potash-bearing Prairie Evaporite units are intermittent within the Williston Basin and thus the mineral composition strongly controls the geochemical signature of formation waters and ability of glaciogenic waters to dissolve evaporites.

3.3 Methods

Groundwater samples were collected into clean 250 mL or 1000 mL HDPE bottles from seeps within mine shafts and mine workings at the Vanscoy, Cory, Allan, and Rocanville potash mines. Dissolved ion concentrations (Cl^-, NO_3^-, F^-, Ca^{2+}, Mg^{2+}, K^+, Na^+, SO_4^{2-}, Br^-, Li^+, Sr^{2+}) were determined by ion chromatography in the Environmental Analytical Laboratory at the Saskatchewan Research Council (Saskatoon, Canada). The $\delta^{18}O$ and δ^2H values were determined using CO_2–H_2O and H_2–H_2O equilibration methods, respectively, at the Saskatchewan Isotope Laboratory (Saskatoon, Canada) and results are reported as the relative difference between the $^{18}O/^{16}O$ and $^2H/^1H$ abundance ratios normalized to Vienna Standard Mean Ocean Water (VSMOW), expressed in per mille (‰) notation. Accuracies of δ^2H and $\delta^{18}O$ are 2‰ and 0.2‰, respectively. Corrections for the salt effect, as outlined by Sofer and Gat (1972; 1975) and Koehler et al. (2013), were applied to the $\delta^{18}O$ and δ^2H values.

The $^{87}Sr/^{86}Sr$ values were analyzed at the Saskatchewan Isotope Laboratory (Saskatoon, Canada) using a Finnigan Triton mass spectrometry instrument in static multi-collection mode, with instrumental mass fractionation that was corrected for $^{86}Sr/^{88}Sr$ of 0.1194. External precision of the $^{87}Sr/^{86}Sr$ measurements performed for these samples was ±8 ppm (2σ) based on repeated measurements of NIST SRM 987, with quality control measurements of 0.710263 ± 0.000010.

The $\delta^{37}Cl$ and $\delta^{81}Br$ values were determined using gas chromatography continuous flow isotope ratio mass spectrometry (GC−CF−IRMS) in the Environmental Isotope Laboratory at the University of Waterloo (Waterloo, Canada). $\delta^{37}Cl$ and $\delta^{81}Br$ values are reported as the relative difference between the $^{37}Cl/^{35}Cl$ and $^{81}Br/^{79}Br$ abundance ratios normalized to the Standard Mean Ocean Chloride (SMOC) and Standard Mean Ocean Bromide (SMOB), respectively, expressed in per mille (‰) notation. Accuracy for both $\delta^{37}Cl$ and $\delta^{81}Br$ is 0.1‰.

Results for dissolved ion concentrations, $\delta^{18}O$ and $\delta^{2}H$, $^{87}Sr/^{86}Sr$, $\delta^{37}Cl$, and $\delta^{81}Br$ may be found in Table B2.

The data is separated into three groups to better understand how basinal fluids evolve over time and space: glaciogenic/meteoric (group 1); mixed brine and glaciogenic (group 2); and paleoevaporated seawater-derived brine (group 3). These groups are defined based on $\delta^{18}O$ values (figure 3−2): group 1:2 boundary occurs at $\delta^{18}O = -14$‰ and group 2:3 boundary is $\delta^{18}O = -5$‰.

Variation in solute and isotope geochemistry may be described using multivariate statistical analyses like Principal Component Analysis (PCA). In short, PCA reduces the dimensionality of the dataset to understand which variable(s) have the largest influence on the dataset (IMDEX, 2019). Data transformation is performed on the solute geochemistry while isotope chemistry is already along a normal distribution. While performing PCA, the sample population was reduced

as a result of fewer samples collected for isotope analysis. PCA was completed via ioGAS software (v. 7.2.1).

3.4 Results and Discussion

A multivariate analysis of the geochemical data supports that there are two main factors controlling the geochemistry of deep groundwaters in the Williston Basin: (1) water origin (glaciogenic or brine), and (2) water-rock interactions (Figure 3−1). While the sample populations were decreased during PCA, Figure 3−1b demonstrates that solute-and-isotope and solute-only PCA have similar relationships and, as such, the isotope sample population is sufficient to draw conclusions.

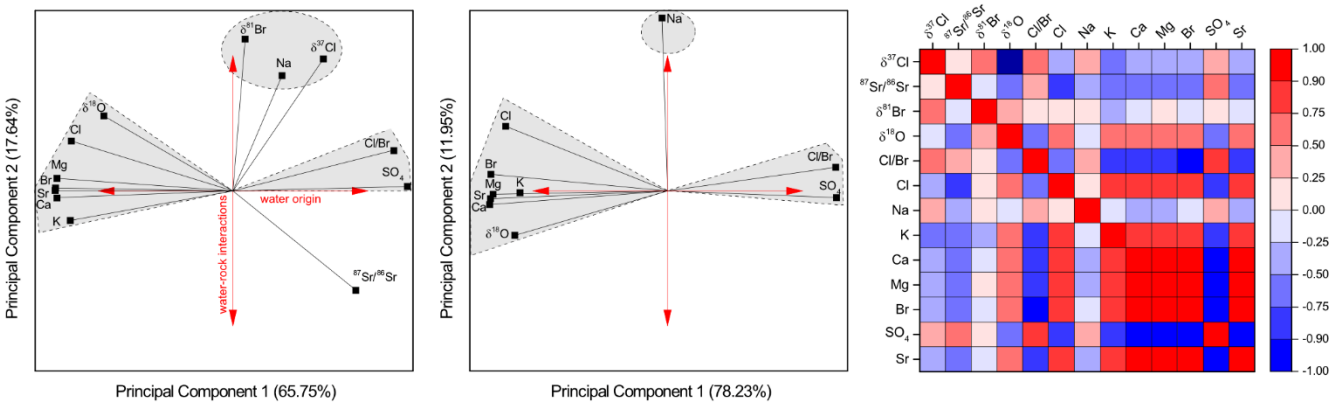

Figure 3−1: Principal Component Analysis and correlative analysis (ioGAS version v. 7.2.1, Table B1) for (a) component 1 and component 2 depicting the relationships between all solute and isotope variables ($n_{samples}$ = 15), and (b) component 1 and component 2 for solute variables only ($n_{samples}$ = 60), and (c) covariance matrix of all solute and isotope variables.

The majority of this data is explained by the water origin and glaciogenic waters are responsible for the majority of salt dissolution, represented by the negative relationship between Cl:Br (molar) ratios and SO_4, and $\delta^{18}O$, Cl, M, Br, Sr, Ca, and K (Figure 3−1, Table B1). However, mineral interactions and mineral composition appear to be an important factor for the novel

isotopes, observed by a cluster for Na, $\delta^{37}Cl$, and $\delta^{81}Br$. $^{87}Sr/^{86}Sr$ values appear to have mixed influence with no clear correlation with other solutes or isotope tracers.

3.4.1 General composition of water sources

Solute composition can be directly linked to salinity and water origin (McIntosh, 2012) and in deep subsurface settings, the composition of Na, Br, and Cl aids in identifying mixing between paleo-evaporated sources and a glaciogenic source via salinity structure (Grasby and Chen, 2005; Tipton, 2018). The sensitive nature of geochemical solutes to mineral precipitation and dissolution reactions makes it difficult to use Na, Cl, or Br to determine a precise mixing line and (or) proportions of mixing between different sources; however, these variables are useful in comparing and contrasting extents of mixing and determining where there has been perturbation and extensive salt dissolution in deep subsurface settings. In addition to solute composition, $\delta^{18}O$ and $\delta^{2}H$ are proven to be valuable in understanding deep subsurface settings altered in the last 1 Ma (Mowat et al., 2021).

The data presented shows widespread values of Cl, Br, and Na observed in the Williston Basin (Figure 3−2). Formation waters that originated from highly evaporated seawater, past halite saturation/precipitation) are enriched in Na, Cl and Br, with Cl:Br values less than seawater (~650) and Na:Cl <0.85 (Connolly et al., 1990) (Figure 3−2c,d). In contrast, glaciogenic waters have relatively low Br concentrations, and high Cl:Br ratios from dissolution of halite, which does not contain appreciable Br. Glaciogenic waters that have dissolved mostly halite salt will also exhibit molar Na:Cl ~ 1. Formation waters in this study have Na:Cl values > 1 with Cl:Br ratios mostly < 500 (figure 3−2d), maybe a result of the glaciogenic groundwaters being relatively fresh with low amounts of halite dissolution.

$\delta^{18}O$ values range between −19.6‰ and +1.8‰, following along the GMWL and to the right, along the evaporation and mixing trend with remnant evaporated paleoseawater-derived brines, respectively. Cory data displays the most glaciogenic signature ($\delta^{18}O = -19.6‰$), as well as the most remnant brine signature of $\delta^{18}O = +1.8‰$. Allan has the largest percent (84%) of $\delta^{18}O$ values indicative of glaciogenic waters ($\delta^{18}O \leq -14‰$) while Rocanville has the greatest percentage of $\delta^{18}O$ values (30%) falling within the range of remnant evaporated paleoseawater-derived brines ($\delta^{18}O \geq -5‰$, Figure 3−2a). In comparison, Allan only has 4% of its $\delta^{18}O$ values classified as evaporated paleoseawater, and Rocanville only has 19% classified as glaciogenic. Mixed waters, where $-14‰ < \delta^{18}O < -5‰$, accounts for approximately 32% of all $\delta^{18}O$ values (Appendix B). These three fluid types – brine, mixed, and glaciogenic – are generally consistent with molar Cl:Br values where there is clear synchronicity between glaciogenic waters which are ^{18}O–depleted with the highest molar Cl:Br value of ~6000 (median = 670), versus evaporated paleoseawater which are ^{18}O-enriched which have a maximum molar Cl:Br value of 1900 (median = 230).

Regionally, groundwater fluid samples collected from Devonian carbonates at Allan and Cory are the most impacted by a glaciogenic source, evidenced by a high proportion of data within glaciogenic range ($\delta^{18}O < -14‰$) and molar Cl:Br values greater than seawater. This suggests that groundwaters at Allan and Cory have been affected more by glacial recharge than Vanscoy or Lanigan groundwaters, which have strong preservation of both glaciogenic and paleoevaporated waters, and (or) Rocanville groundwaters where there is minor glaciogenic perturbation based on Na, Cl, Br, and $\delta^{18}O$ data. These observations may be explained by multiple scenarios, including: (1) lack of extensive glacial flushing in the area of Rocanville and the center of the basin in comparison to Allan or Cory, (2) Rocanville groundwaters have not been perturbed and flushed as

recently as other locations, or (3) Rocanville did not experience as much salt dissolution due to local and regional salt discontinuity. Our results identify flow paths throughout the Williston Basin, concluding that there has likely been a greater flushing towards the center of the Williston

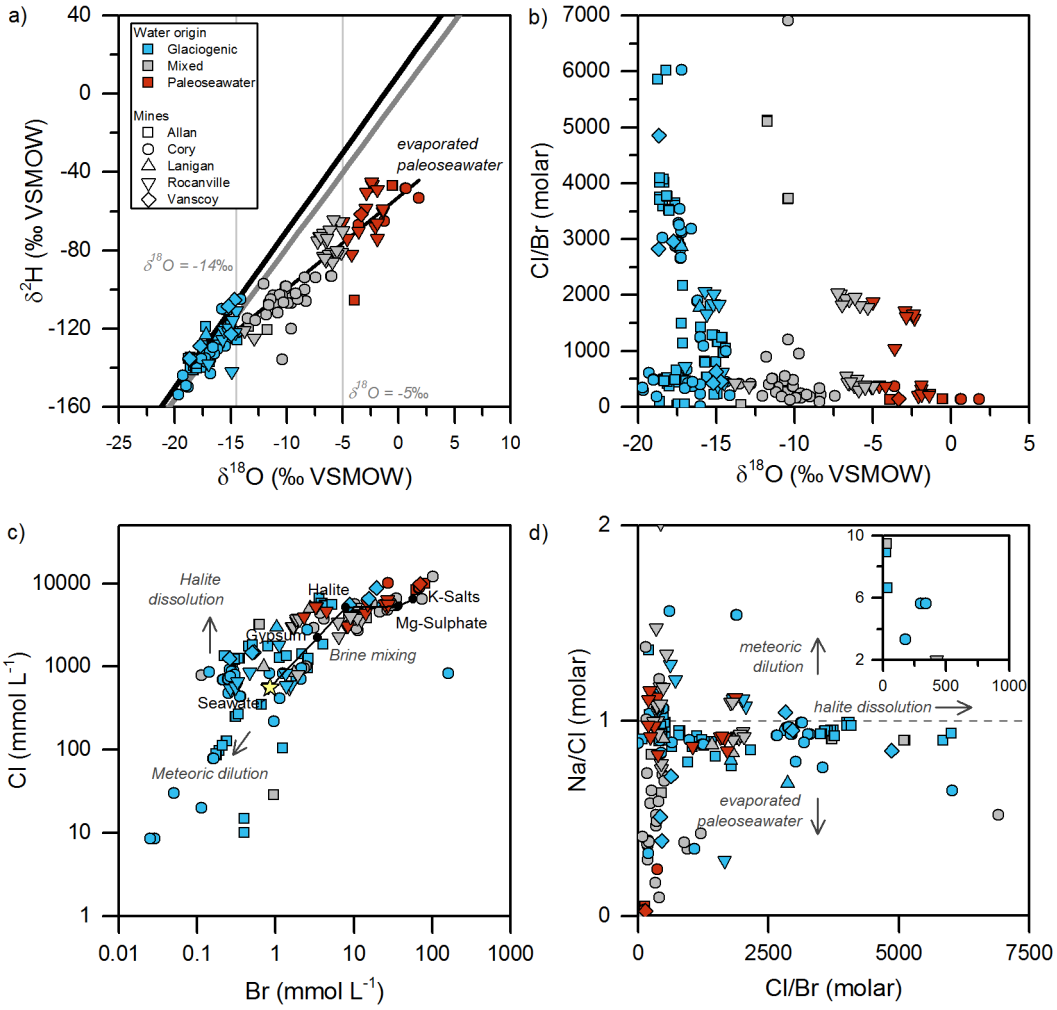

Figure 3−2: Geochemical results for all available data, attributed by water origin (color) and mine (shape) for: (a) $\delta^{18}O$ versus $\delta^{2}H$ values relative to the global (black) and local (grey) meteoric water lines, (b) $\delta^{18}O$ versus Cl:Br values, (c) molar Br versus Cl with the seawater evaporation trajectory, and (d) Cl:Br values versus molar Na:Cl values.

Basin along the north to northeast in comparison to the eastern margin. The east-northeastern margin experienced glacial meltwater recharge; however it is possible that it has not been as

extensively flushed into the center of the basin. These observations have also been identified via solute composition and hydraulic head maps in Tipton (2018) and 1−D profile modeling (Mowat et al., 2021), and they are likely a function of differences in permeability at a regional level resulting in differences in timing and intensity of salt dissolution.

3.4.2 Strontium Isotopes ($^{87}Sr/^{86}Sr$)

$^{87}Sr/^{86}Sr$ signatures are well−described in the literature throughout geologic history (McArthur et al., 2012) and, although very deep subsurface paleoevaporated brines may experience $^{87}Sr/^{86}Sr$ overprinting by migration and (or) mixing interaction, a general trend between water−origin and mixing reactions has been observed in $^{87}Sr/^{86}Sr$ values in sedimentary basins which experienced glacial recharge and salt dissolution (McNutt et al., 1987; Connolly et al., 1990; Birks et al., 2019; Marza et al., 2022). Particularly, groundwater that is distinctly different from the paleoevaporated brine source geochemistry and surrounding host rocks is clear evidence that there has been a long fluid migration to the present location. Chaudhuri and Clauer (1993) identify fluid migration and dilution as a main source of radiogenic signatures in sedimentary basins as a result of water−rock interactions with marine carbonate and sulfate minerals during the fluid transport process, such as the fluid pathways glaciogenic waters have taken in the Williston Basin.

Results from this study indicate that evaporated paleoseawater are less radiogenic with lower $^{87}Sr/^{86}Sr$ values (median = 0.7083, maximum = 0.7084), while glaciogenic sources are more radiogenic with higher $^{87}Sr/^{86}Sr$ values (median = 0.7087, maximum = 0.7088) because of water-rock interactions. Due to lower data density, evaluating $^{87}Sr/^{86}Sr$ signatures at a stratigraphic level proves to be difficult – however, observed correlative analysis between solute variables and

$^{87}Sr/^{86}Sr$ values demonstrates that molar Cl:Br values and SO_4 are reasonable options for comparing glaciogenic and evaporated paleoseawater.

Table 1: Minimum, maximum, and median values of $^{87}Sr/^{86}Sr$ for glaciogenic waters, mixed, and paleoseawater.

	$^{87}Sr/^{86}Sr$		
	Glaciogenic	Mixed	Paleoseawater
$n_{samples}$	9	5	2
Minimum	0.70813	0.70806	0.70811
Maximum	0.70881	0.70818	0.70844
Median	0.70865	0.70810	0.70828

$^{87}Sr/^{86}Sr$ versus molar Cl:Br ratios demonstrate a positive relationship until approximately Cl:Br ~ 1500 where $^{87}Sr/^{86}Sr$ values reach a maximum of 0.7078 while there is still a steady increase in molar Cl:Br. Group 1 locations with the most radiogenic $^{87}Sr/^{86}Sr$ values (Cory, Allan) also have the greatest salt dissolution with high molar Cl:Br values indicating intensive water-rock interactions and dissolution of low-evaporitic sulfate-rich salts (anhydrite, gypsum; high SO_4 concentrations). The Rocanville sample (Figure 3−3a, 3−3b) is the least radiogenic where the effects of salt dissolution also appear lowest based on solute geochemistry. These results suggest that relatively radiogenic Sr is being released to formation waters during dissolution of Ca-bearing evaporites.

Maximum $^{87}Sr/^{86}Sr$ values for the suite of Devonian carbonates in the Williston Basin is 0.7082 (McArthur et al., 2012) which agrees with the evaporated paleoseawater values in this study (Figure 3−3). However, many of the glaciogenic group 1 samples – expected to be more radiogenic – have low $^{87}Sr/^{86}Sr$, evidence that a glaciogenic source dissolving radiogenic minerals is not the only factor in estimating $^{87}Sr/^{86}Sr$ values. Principal component analysis verifies that there

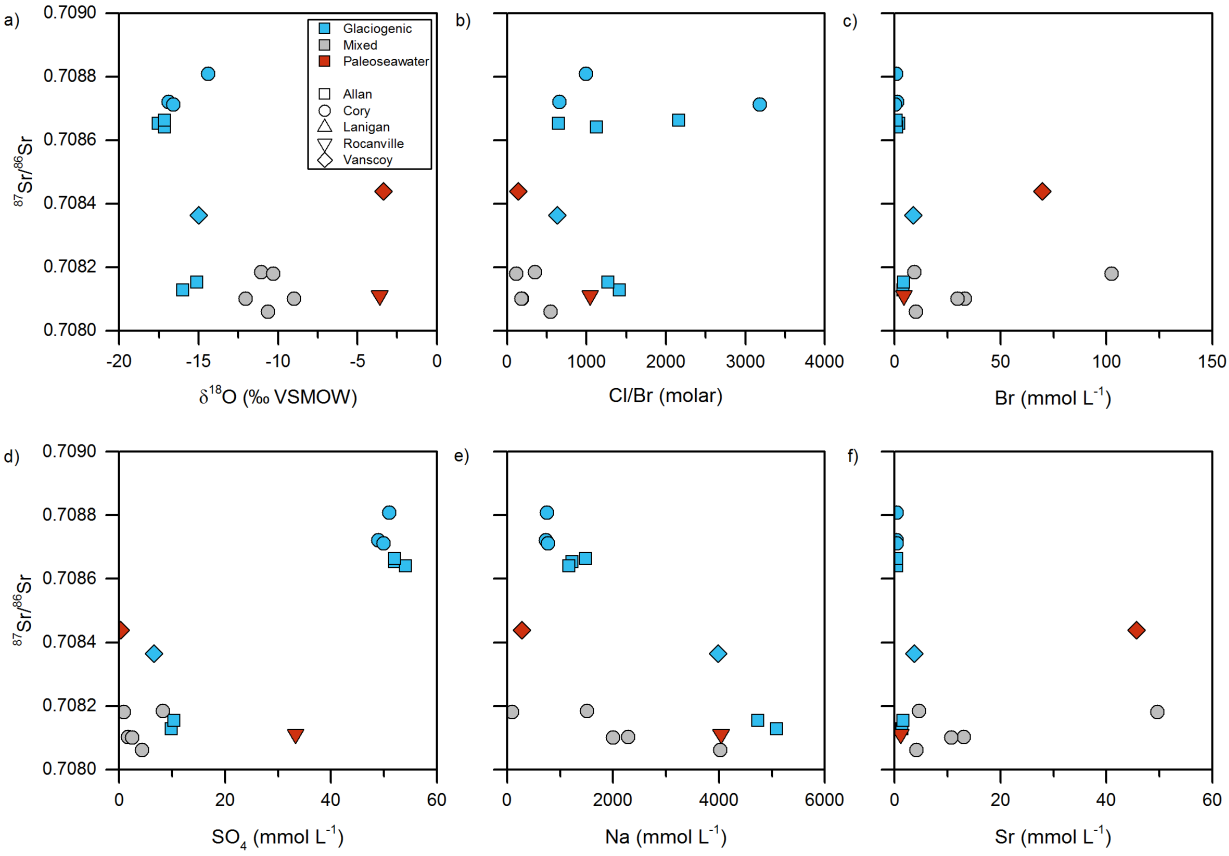

Figure 3−3: Geochemical results attributed by water origin (color) and mine (shape) for $^{87}Sr/^{86}Sr$ versus (a) $\delta^{18}O$, (b) Cl/Br, (c) Br, (d) SO_4, (e) Na, and (f) Sr.

is no single variable that can explain $^{87}Sr/^{86}Sr$ ratios (Figure 3−1), and that $^{87}Sr/^{86}Sr$ is dependent on both water origin and intensity of salt dissolution and water-rock interactions.

3.4.3 Chlorine and Bromine Isotopes ($\delta^{37}Cl$ and $\delta^{81}Br$)

The data for $\delta^{37}Cl$ and $\delta^{81}Br$ reveal synonymous patterns between water types: glaciogenic waters exhibit a large range in values ($-0.155 < \delta^{37}Cl < 0.352$ and $0.157 < \delta^{81}Br < 1.649$) while evaporated paleoseawaters have less variance in values ($-0.096 < \delta^{37}Cl < 0.052$ and $0.685 < \delta^{81}Br < 1.069$) (Table 1).

	$\delta^{37}Cl$			$\delta^{81}Br$		
	Glaciogenic	Mixed	Paleoseawater	Glaciogenic	Mixed	Paleoseawater
$n_{samples}$	*24*	*6*	*2*	*24*	*6*	*2*
Minimum	-0.155	-0.323	-0.096	0.157	0.236	0.685
Maximum	0.352	0.219	0.200	1.649	0.968	1.069
Median	0.062	-0.125	0.052	0.529	0.392	0.877

Table 2: Minimum, maximum, and median values of $\delta^{37}Cl$ and $\delta^{81}Br$ for glaciogenic waters, mixed, and paleoseawater.

It is challenging to conclude trends between locations due to low sample density; however, there is a notable negative and positive correlation between water origin versus $\delta^{37}Cl$ and $\delta^{81}Br$ values, respectively. The main correlations based on water origin (groups 1–3) between $\delta^{37}Cl$ and $\delta^{81}Br$ isotopes with other variables based on PCA include: $\delta^{37}Cl$ versus molar Cl:Br, Cl, $\delta^{81}Br$, and SO_4, and $\delta^{81}Br$ versus K. Principal component analysis indicates that halite dissolution is the driving factor controlling $\delta^{37}Cl$ and $\delta^{81}Br$ values: there is a positive correlation with Na, and a positive correlation with molar Cl:Br due to these variables being largely dependent on the extent of salt dissolution and (or) variation of halite that is being dissolved (e.g. where Br has been substituted into the mineral lattice in the latest stages of mineral precipitation (McCaffrey et al., 1987)) (Figure 3−1, Figure 3−4).

$\delta^{37}Cl$ values and molar Cl:Br ratios have the strongest affinity together until Cl:Br ~ 4000, and then the trend reverses. The point of inflection for molar Cl:Br values indicates the dissolution of the most concentrated halite (e.g. dissolution of halite which formed in the latest stages of mineral precipitation and contain Br), Mg-salts, and K-salts (Figure 3−4b, Figure 3−2c). The influence of water origin is highlighted here, as glaciogenic groundwater will have the greatest ability to dissolve salts while paleoevaporated brines may already be at (or near) saturation; in this

case, it is positively supported by a weak negative relationship between $\delta^{18}O$ and $\delta^{37}Cl$ (Figure 3−1, Figure 3−4g).

The values of $\delta^{81}Br$ suggest that they are dependent on water origin, although there is no correlation observed between $\delta^{81}Br$ and the rest of the variables. The strongest correlation is between $\delta^{81}Br$ and K, while there is a weak correlation between $\delta^{81}Br$ and $\delta^{18}O$ where there is a general increase of $\delta^{81}Br$ based on water origin (Figure 3−4g, 4h).

Overall, there is little known about the effects on $\delta^{37}Cl$ and $\delta^{81}Br$ when mixing groundwater sources, although some research has hypothesized the possible patterns relate to isotope fractionation in paleo-evaporated sources. Literature states that during large scale evaporation and mineral precipitation, $\delta^{37}Cl$, $\delta^{81}Br$, and relative molar Cl:Br values are recorded in halite and other Cl and Br rich minerals (McCaffrey et al., 1987; Eggenkamp et al., 1995; Shouakar-Stash, 2008; Stotler et al., 2010), and the remnant paleoevaporated groundwater will exhibit enriched $\delta^{37}Cl$ and $\delta^{81}Br$ values. During glacial meltwater perturbation and major halite salt dissolution, ^{37}Cl-depleted and $\delta^{81}Br$-depleted signatures preserved in halite will be recorded in the glaciogenic and mixed groundwater. The Williston Basin is host to extensive evaporative minerals beyond halite, therefore knowledge of water origin is helpful to understand the effects on $\delta^{37}Cl$ and $\delta^{81}Br$ geochemistry.

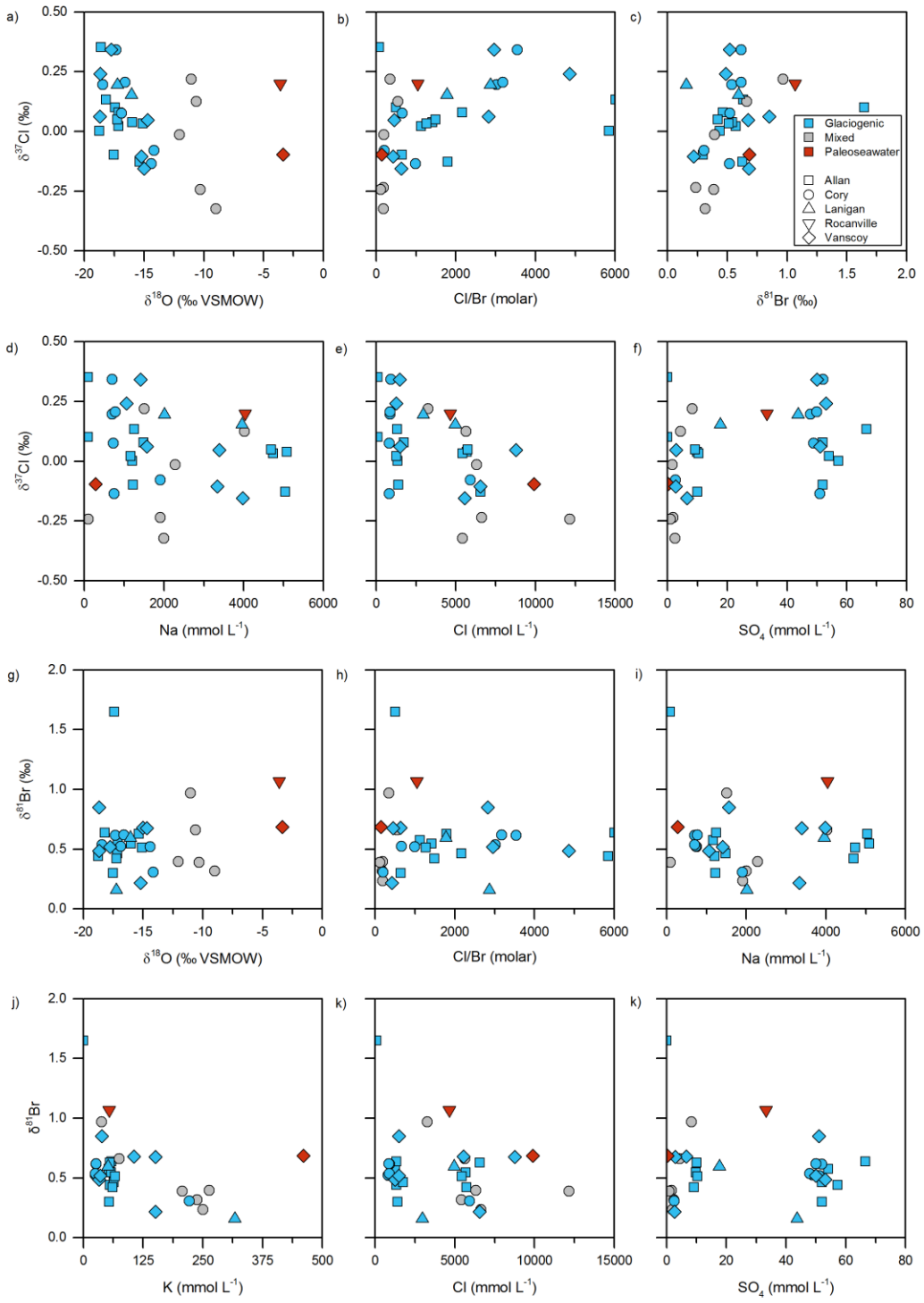

Figure 3−4: Geochemical results attributed by water origin (color) and mine (shape) for $\delta^{37}Cl$ versus (a) $\delta^{18}O$, (b) Cl/Br, (c) $\delta^{81}Br$, (d) Na, (e) Cl, and (f) SO_4, and $\delta^{81}Br$ versus (g) $\delta^{18}O$, (h) Cl/Br, (i) Na, (j) K, (k) Cl, and (l) SO_4.

3.5 Conclusions

A combination of new isotope and solute geochemistry of formation waters in the Williston Basin helps inform the differences between glaciogenic and evaporated paleoseawater-derived waters at depth. Although mixing and water−rock interactions can present challenges by modifying fluid chemistry and obscuring sources, this study combines multiple tracers to better understand novel isotope fractionation processes. The results support a continuous recharge belt along the north-to-eastern margins of the Williston Basin (Mowat et al., 2021), and shows that strong glacial recharge signatures are preserved deep into the Williston Basin.

Comparing isotope systems to solute and stable isotope geochemistry informs trends that contribute to fractionation of $^{87}Sr/^{86}Sr$, $\delta^{37}Cl$, and $\delta^{81}Br$. Results show the importance of variation in salt and mineral composition on the concentrations and values of molar Cl:Br, $\delta^{37}Cl$, and $\delta^{81}Br$, or the sensitivity of $^{87}Sr/^{86}Sr$ values to overprinting and water-rock interaction processes. A combination of statistical and correlative analysis tools established the variation in geochemistry between glaciogenic and brine sources. Application of this multi-tracer approach using large datasets and data mining for other sedimentary basins may provide further insights into the signatures of novel isotope tracers and the mixing and evolution of multiple water sources.

3.6 Acknowledgments and Data

Funding was provided to G. Ferguson by Global Water Futures and the University of Saskatchewan Centennial Engagement Chair. Additional support is awarded to A. Mowat from the Natural Sciences and Engineering Research Council of Canada (NSERC) Canadian Graduate Scholarship – Master's Program (NSERC CGS-M), the NSERC Postgraduate Scholarship – Doctoral (NSERC PGS-D) Program, the University of Saskatchewan Dean's Scholarship, and the

Saskatchewan Queen Elizabeth II Centennial Aboriginal Scholarship. All data included in this manuscript are included in Appendix B, and (or) at the following DOI: 10.5281/zenodo.7749457

CHAPTER 4: CONCLUSION

Glacial recharge has impacted sedimentary basins across the northern hemisphere and the Williston Basin in the Western Canada Sedimentary Basin is no exception. Massive regions of salt dissolution along the northeast to east margin of the Williston Basin has resulted in vastly different geochemical signatures of formation waters and major changes to energy and mineral resources including oil, gas, and potash potential.

This thesis examined the effects of glaciogenic recharge to deep subsurface aquifers in the Williston Basin and approximated the age of recharge perturbations using an interdisciplinary approach between geochemistry, geology, and computational modeling. Here, we conclude that glaciogenic recharge occurred during two separate time periods, 75 to 150 ka and 300 ka, to the northcentral regions of the Williston Basin. Spatial reconstruction between observed trends in the Williston Basin indicated that there was a much larger impact by subglacial recharge along the north to northeast margin than previously anticipated.

Geochemistry in this deep, isolated aquifer system of the Williston Basin is differentiated into two categories: glaciogenic recharge and paleoevaporated brines. Strong trends are observed for Molar Cl:Br, $\delta^{18}O$, and $\delta^{2}H$ values, and moderate trends are observed for $^{87}Sr/^{86}Sr$, $\delta^{37}Cl$, and $\delta^{81}Br$ values despite a smaller sample density and less literature to describe the trends. Qualitative tools, like statistical and correlative analysis, and quantitative tools were used to discern the main influences to brine geochemistry in the data set: water-rock interactions and water origin. In conclusion, this study provided new insights into the timing and variability in recharge of

glaciogenic waters and the geochemical variation in solutes and isotope systems between paleoevaporated and glaciogenic sourced groundwaters in the Williston Basin.

In anticipation of further research, additional samples should be collected to increase the data density for solute geochemistry, prioritizing additional sampling for novel isotopes included in this study to more rigorously constrain the isotope fractionation, mixing, and water-rock interactions influencing these variables. Sample collection and analysis for noble gases (^{4}He and ^{81}Kr) would also be useful to help better constrain the residence time of groundwaters and timing of subglacial recharge.

REFERENCES

Bachu, S. and Hitchon, B. (1996). Regional-scale flow of formation waters in the Williston Basin. *AAPG Bulletin, 80*(2), 248–264. https://doi.org/10.1306/64ED87A0-1724-11D7-8645000102C1865D

Bense, V.F., and Person, M.A. (2008). Transient hydrodynamics within intercratonic sedimentary basins during glacial cycles. *Journal of Geophysical Research: Earth Surface, 113*(4), 1–17. https://doi.org/10.1029/2007JF000969

Birks, S.J., Fennell, J.W., Gibson, J.J., Yi, Y., Moncur, M.C., and Brewster, M. (2019) Using regional datasets of isotope geochemistry to resolve complex groundwater flow and formation connectivity in northeastern Alberta, Canada. *Applied Geochemistry, 101,* 140-159. https://doi.org/10.1016/j.apgeochem.2018.12.013

Boudreau, B.P. (1996). The diffusive tortuosity of fine-grained unlithified sediments. *Geochimica et Cosmochimica Acta, 60*(16), 3139-3142. https://doi.org/10.1016/0016-7037(96)00158-5

Boudreau, B.P., and Meysman P.J.R. (2006). Predicted tortuosity of muds. *Geology, 34*(8), 693-696. https://doi.org/10.1130/G22771.1

Boulton, G.S., Caban, P.E., and Gijssel, Van K. (1995) Groundwater flow beneath ice sheets: Part 1 – Large scale patterns. *Quaternary Science Reviews, 14,* 545-562. https://doi.org/10.1016/0277-3791(95)00039-R

Boulton, G.S., Caban, P.E., Gijssel, Van K., Leijnse, A., Punkari, M., and van Weert, F.H.A (1996) The impact of glaciation on the groundwater regime of Northwest Europe. *Global and Planetary Change, 12,* 397-413. https://doi.org/10.1016/0921-8181(95)00030-5

Chaudhuri, S., and Clauer, N. (1993) Strontium isotopic compositions and potassium and rubidium contents of formation waters in nsediemtnary basins: Clues to the origin of the solutes. *Geochemica et Cosmochimica Acta, 57,* 429−437. https://doi.org/10.1016/0016-7037(93)90441-X

Christiansen, E.A., and Sauer, E.K. (2001). Stratigraphy and structure of a Late Wisconsinan salt collapse in the Saskatoon Low, south of Saskatoon, Saskatchewan, Canada: an update.

Canadian Journal of Earth Sciences, *38*(11), 1601–1613. https://doi.org/10.1139/cjes-38-11-1601

Christiansen, E.A., Gendzwill, D.J., and Meneley, W.A. (1982). Howe lake: a hydrodynamic blowout structure. *Canadian Journal of Earth Sciences*, *19*(6), 1122–1139. https://doi.org/10.1139/e82-097

Cloutier V., Lefebvre R., Savard M.M., Bourque D., and Therrien R. (2006). Hydrogeochemistry and groundwater origin of the Basses-Laurentides sedimentary rock aquifer system, St. Lawrence Lowlands, Que´bec, Canada. *Hydrogeology Journal*, *14,* 573–590. https://doi.org/10.1007/s10040-005-0002-3

Connolly, C.A., Walter, L.M., Baadsgaard, H., and Longstaffe, F.J. (1990) Origin and evolution of formation waters, Alberta Basin, Western Canada Sedimentary Basin – 1. Chemistry. *Applied Geochemistry, 5,* 375-395.

Edmunds, W.M., Milne, C.J. (2001). Palaeowaters in Coastal Europe: Evolution of Groundwater since the Late Pleistocene. Geological Society, London, Special Publications, *189*. https://doi.org/10.1144/GSL.SP.2001.189

Eggenkamp, H.G.M., Kreulen, R., and Koster van Groos, A.F. (1995) Chlorine stable isotope fractionation in evaporites. *Geochimica et Cosmochemica Acta, 59(24),* 5169-5175. https://doi.org/10.1016/0921-8181(95)00030-5

Ehlers, J., and Gibbard, P (2008). Extent and chronology of Quaternary glaciation. *Episodes,* 31(2), 211-218. https://doi.org/10.18814/epiiugs/2008/v31i2/004

Ferguson, G., Betcher, R.N., & Grasby, S.E. (2007). Hydrogeology of the Winnipeg formation in Manitoba, Canada. *Hydrogeology Journal*, *15*(3), 573–587. https://doi.org/10.1007/s10040-006-0130-4

Ferguson, G. and Jasechko, S. (2015). The isotopic composition of the Laurentide Ice Sheet and fossil groundwater. *Geophysical Research Letters*, *42*(12), 4856–4861. https://doi.org/10.1002/2015GL064106

Ferguson, G., McIntosh, J.C., Grasby, S.E., Hendry, M.J., Jasechko, S., Lindsay, M.B.J., & Luijendijk, E. (2018). The Persistence of Brines in Sedimentary Basins. *Geophysical Research Letters*, *45*(10), 4851–4858. https://doi.org/10.1029/2018GL078409

Gerber, C., Vaikmäe, R., Aeschbach, W., Babre, A., Jiang, W., Leuenberger, M., … and Purtschert, R. (2017). Using ^{81}Kr and noble gases to characterize and date groundwater and brines in the Baltic Artesian Basin on the one-million-year timescale. *Geochimica et Cosmochimica Acta*, *205*, 187–210. https://doi.org/10.1016/j.gca.2017.01.033

Grasby, S.E., and Betcher, R.N. (2002). Regional hydrogeochemistry of the carbonate rock aquifer, southern Manitoba. *Canadian Journal of Earth Sciences*, *39*(7), 1053–1063. https://doi.org/10.1139/e02-021

Grasby, S.E., and Chen, Z. (2005). Subglacial recharge into the Western Canada Sedimentary Basin - Impact of Pleistocene glaciation on basin hydrodynamics. *Bulletin of the Geological Society of America*, *117*(3–4), 500–514. https://doi.org/10.1130/B25571.1

Grasby, S.E., Hutcheon, I., and Krouse, H.R. (2000). The influence of water-rock interaction on the chemistry of thermal springs in western Canada. *Applied Geochemistry*, *15*, 439-454. https://doi.org/10.1016/S0883-2927(00)00020-2

Hendry, M.J., Barbour, S.L., Novakowski, K., and Wassenaar, L.I. (2013). Paleohydrogeology of the Cretaceous sediments of the Williston Basin using stable isotopes of water. *Water Resources Research*, *49*(8), 4580–4592. https://doi.org/10.1002/wrcr.20321

Hendry, M.J., Barbour, S.L., Boldt-Leppin, B., Reifferscheid, L., and Wassenaar, L.I. (2009). A comparison of laboratory and field based determinations of molecular diffusion coefficients in a low permeability geologic medium. *Environmental Science and Technology*, *43*(17), 6730–6736. https://doi.org/10.1021/es901036p

Hendry, M.J., and Harrington, G.A. (2014). Comparing vertical profiles of natural tracers in the Williston Basin to estimate the onset of deep aquifer activation. *Water Resources Research*, *50*(8), 6496–6506. https://doi.org/10.1002/2014WR015652

Hitchon, B. (1969a). Fluid flow in the Western Canada Sedimentary Basin: 2. Effect of topography. *Water Resources Research*, *5*(1), 186–195. https://doi.org/10.1029/WR005i001p00186

Hitchon, B. (1969b). Fluid flow in the Western Canada Sedimentary Basin: 2. Effect of geology. *Water Resources Research, 5*(2), 460–469. https://doi.org/10.1029/WR005i002p00460

Holter, M.E. (1969) The Middle Devonian Prairie Evaporite of Saskatchewan. *Saskatchewan Department of Mineral Resources, Report no. 123.*

IHS Energy (2017). IHS Accumap *in* Commercial database, IHS Energy.

Jasechko, S. (2019) Glocal Isotope Hydrogeology—Review. *Reviews of Geophysics, 57,* 835-965. https://doi.org/10.1029/2018RG000627

Jensen, G.K.S., Rostron, B.J., Duke, M.J.M., & Holmden, C. (2006) Chemical profiles of formation waters from potash mine shafts, Saskatchewan. *Summary of Investigations, 1*, 1-8.

Kent, D.M., and Christopher, J.E. (1994). Geological History of the Williston Basin and Sweetgrass Arch. In G.D. Mossop, and I. Shetsen, (Eds.), *Geological Atlas of the Western Canada Sedimentary Basin* (pp. 421–430). Canadian Society of Petroleum Geologists and Alberta Research Council. Retrieved from https://ags.aer.ca/reports/atlas-of-the-western-canada-sedimentary-basin.html

Kloppman, W., Negrel., P., Casanova, J., Klinge, H., Schelkes, K., Guerrot, C. (2001) Halite dissolution derived brines in the vicinity of a Permian salt dome (N German Basin): Evidence from boron, strontium, oxygen, and hydrogen isotopes. *Geochimica et Cosmochimica Acta*, *65*(22), 4087-4101. https://doi.org/10.1016/S0016-7037(01)00640-8

Koehler, G., Wassenaar, L.I., and Hendry, J. (2013). Measurement of stable isotope activities in saline aqueous solutions using optical spectroscopy methods. *Isotopes in Environmental and Health Studies*, *49*(3), 378–386. https://doi.org/10.1080/10256016.2013.815183

Lemieux, J.-M., Sudicky, E.A., Peltier, W.R., Tarasov, L. (2008) Simulating the impact of glaciations on continental groundwater flow systems: 2. Model application to the

Wisconsinian glaciation over the Canadian landscape. *Journal of Geophysical Research*, 113(F03018). https://doi.org/10.1029/2007JF000929

Lemieux, J.-M. (2011) Review: The potential impact of underground geological storage of carbon dioxide in deep saline aquifers on shallow groundwater resources. *Hydrogeology Journal, 19,* 757-778. http://doi.org/10.1007/s10040-011-0715-4

Marsh, A. and Love, M. (2014). Regional Stratigraphic Framework of the Phanerozoic in Saskatchewan; Saskatchewan Phanerozoic Fluids and Petroleum Systems Project; Sask. Ministry of Energy and Resources, Saskatchewan Geological Survey.

Martini, A.M., Walter, L.M., and McIntosh, J.C. (2008). Identification of microbial and thermogenic gas components from Upper Devonian black shale cores, Illinois and Michigan basins. *American Association of Petroleum Geologists Bulletin*, *92*(3), 327–339. https://doi.org/10.1306/10180706037

Marza, M., Mowat, A., Jellicoe, K., Ferguson, G., & McIntosh, J. (2022) Evaluation of strontium isotope tracers of produced water sources from multiple stacked reservoirs in Appalachian, Williston and Permian basins. *Journal of Geochemical Exploration, 232*, 1068-1087. https://doi.org/10.1016/j.gexplo.2021.106887

Mazor, E., and Bosch, A. (1987). Noble gases in formation fluids from deep sedimentary basins: a review. *Applied Geochemistry*, *2*(5–6), 621–627. https://doi.org/10.1016/0883-2927(87)90014-X

McArthur, J.M., Howarth, R.J., & Shields, G.A. (2012) Strontium Isotope Stratigraphy. *The Geologic Time Scale 2012, 1–2,* 127–144. https://doi.org/10.1016/B978-0-444-59425-9.00007-X

McCaffrey, M.A., Lazar, B., & Holland, H.D. (1987). The evaporation path of seawater and the coprecipitation of Br^- and K^+ with halite. *Journal of Sedimentary Petrology, 57(5),* 928-938. https://doi.org/10.1306/212f8cab-2b24-11d7-8648000102c1865d

McIntosh, J. C., and Walter, L. M. (2006). Paleowaters in Silurian-Devonian carbonate aquifers: Geochemical evolution of groundwater in the Great Lakes region since the Late Pleistocene.

Geochimica et Cosmochimica Acta, *70*(10), 2454–2479. https://doi.org/10.1016/j.gca.2006.02.002

McIntosh, J.C., Garven, G., and Hanor, J.S. (2011). Impacts of Pleistocene glaciation on large-scale groundwater flow and salinity in the Michigan Basin. *Geofluids*, *11*(1), 18–33. https://doi.org/10.1111/j.1468-8123.2010.00303.x

McIntosh, J.C., Schlegel, M.E., and Person, M. (2012). Glacial impacts on hydrologic processes in sedimentary basins: Evidence from natural tracer studies. *Geofluids*, *12*(1), 7–21. https://doi.org/10.1111/j.1468-8123.2011.00344.x

McIntosh J.C., Walter, L.M., Martini, A.M. (2002). Pleistocene recharge to mid-continent basins: effects on salinity structure and microbial gas generation. *Geochimica et Cosmochimica Acta, 66*(10), 1681–1700. https://doi.org/10.1016/S0016-7037(01)00885-7

McNutt, R.H., Frape, S.K., & Dollar, P. (1987) A strontium, oxygen and hydrogen isotopic composition of brines, Michigan and appalachian basins, Ontario and Michigan. *Applied Geochemistry, 2(5–6),* 495-505. https://doi.org/10.1016/0883-2927(87)90004-7

Mowat, A.C., Francis, D.J., Mcintosh, J.C., Lindsay, M.B.J., and Ferguson, G. (2021) Variability in timing and transport of Pleistocene meltwater recharge to regional aquifers. *Geophysical Research Letters, 48*, 1-10. https://doi.org/10.1029/2021GL094285

Palombi, D. D. (2008). Regional Hydrogeological Characterization of the Northeastern Margin in the Williston Basin (Master of Science, thesis). University of Alberta, Edmonton, Canada.

Person, M., McIntosh, J., Bense, V., and Remenda, V.H. (2007). Pleistocene hydrology of North America: The role of ice sheets in reorganizing groundwater flow systems. *Reviews of Geophysics*, *45*(3), 1–28. https://doi.org/10.1029/2006RG000206

Person, M. (2007). Pleistocene Hydrogeology of the Atlantic Continental Shelf, New England. In P.G. Knight. (Ed). *Glacier Science and Environmental Change*, *11*, 68–70. https://doi.org/10.1002/9780470750636.ch13

Phillips, F.M., and Castro, M.C. (2013). Groundwater Dating and Residence-Time Measurements. In H.D. Holland, and K.K. Turekian (Eds.). *Treatise on Geochemistry: Second Edition*, *7*, 361–400. https://doi.org/10.1016/B978-0-08-095975-7.00513-1

Rostron, B.J., & Holmden, C. (2000). Fingerprinting formation waters using stable isotopes, Midale Area, Williston Basin, Canada. *Journal of Geochemical Exploration, 69–70,* 219-223. https://doi.org/10.1016/S0375-6742(00)00024-8

Schlegel, M.E., Zhou, Z., McIntosh, J.C., Ballentine, C.J., and Person, M.A. (2011). Constraining the timing of microbial methane generation in an organic-rich shale using noble gases, Illinois Basin, USA. *Chemical Geology*, *287*(1–2), 27–40. https://doi.org/10.1016/j.chemgeo.2011.04.019

Schmeling, E.E. (2014). *Characterization of the hydrogeology and solute transport in a geologically complex, fractured, late-Cretaceous shale, Fort a la Corne kimberlite field, Saskatchewan, Canada* (Master of Science, thesis). University of Saskatchewan, Saskatoon, Canada.

Shouakar-Stash, O. (2008). Evaluation of stable chlorine and bromine isotopes in sedimentary formation fluids. (Doctor of Philosophy, dissertation). University of Waterloo, Waterloo, Canada.

Siegel, D.I. (1991). Evidence for dilution of deep, confined groundwater by vertical recharge of isotopically heavy Pleistocene water. *Geology, 19,* 433–436. https://doi.org/10.1130/0091-7613(1991)019<0433:EFDODC>2.3.CO;2

Sofer, Z., and Gat, J.R. (1972). Activities and concentrations of O-19 in concentrated aqueous salt solutions: Analytical and geophysical implication. *Earth and Planetary Science Letters*, *15,* 232–238. https://doi.org/10.1016/0012-821X(72)90168-9

Sofer, Z., and Gat, J.R. (1975). The isotope composition of evaporating brines: Effect of the isotopic activity ratio in saline solutions. *Earth and Planetary Science Letters*, *26*(2), 179–186. https://doi.org/10.1016/0012-821X(75)90085-0

Stotler, R.L., Frape, S.K., and Shouakar-Stash, O. (2010). An isotopic survey of δ^{81}Br and δ^{37}Cl of dissolved halides in the Canadian and Fennoscandian Shields. *Chemical Geology, 274(1–2),* 38-55. https://doi.org/10.1016/j.chemgeo.2010.03.014

Tipton, K.J.L. (2018). *Variations in salinity structure in Saskatchewan's Devonian carbonates* (Master of Science, thesis). University of Saskatchewan, Saskatoon, Canada.

Wittrup, M.B., and Kyser, T.K. (1990). The petrogenesis of brines in Devonian potash deposits of western Canada. *Chemical Geology*, *82*, 103–128. https://doi.org/10.1016/0009-2541(90)90077-K

APPENDIX

APPENDIX A

Table A1: Compilation of data.

Source	Mine	Formation/ Group	Aquifer/ Aquitard	Depth (m BG)	δ18O	δD	Cl (mg L-1)	Na (mg L-1)	Br (mg L-1)
This study	Allan	Bearpaw		76	-17.4	-135.8	3460	2170	15.4
This study	Allan	Bearpaw		76	-18.6	-134.7	3700	2170	100
Jensen et al. (2006)	Allan	Cret. Shales		98	-18.3	-140.6	3021	2015	14
Jensen et al. (2006)	Allan	Cret. Shales		104	-18.1	-138.9	3181	1959	14
Nutrien internal database	Allan	Cret. Shales		122	-17.5	-129	354	2050	32
Wittrup and Kyser (1990)	Allan	Cret. Shales		122	-17.5	-129	354	2050	32
Jensen et al. (2006)	Allan	Cret. Shales		149	-17.2	-133.2	4529	2689	19
Wittrup and Kyser (1990)	Allan	Cret. Shales		158	-17.4	-136	530	2280	32
Nutrien internal database	Allan	Cret. Shales		159	-17	-136	530	2280	32
Jensen et al. (2006)	Allan	Cret. Shales		183	-17.4	-135.2	3978	2494	17
Jensen et al. (2006)	Allan	Cret. Shales		290	-15.7	-121.3	8784	5396	25
Jensen et al. (2006)	Allan	Cret. Shales		332	-15	-118.5	9519	5712	27
Wittrup and Kyser (1990)	Allan	Cret. Shales		341	-13.4	-119	1020	6250	76
Jensen et al. (2006)	Allan	Cret. Shales		378	-15.6	-120.5	12364	7948	53
Jensen et al. (2006)	Allan	Watrous		610	-10.4	-105.7	37863	22193	23
Nutrien internal database	Allan	Watrous		610	-18.1	-138	26700	15500	148
Wittrup and Kyser (1990)	Allan	Birdbear		655	-17.4	-136	31000	19800	160
This study	Allan	Birdbear		669	-17.5	-135	50200	28200	174
This study	Allan	Birdbear		669	-18.7	-135.5	47800	27800	18.4
This study	Allan	Birdbear		672	-17.1	-134.3	45100	26900	90
This study	Allan	Birdbear		672	-18.2	-136.4	47500	28800	17.8
Jensen et al. (2006)	Allan	Duperow	Seward	681	-18.3	-141.3	42714	27391	24
Jensen et al. (2006)	Allan	Duperow	Seward	683	-18.4	-140.1	44482	27219	28
Jensen et al. (2006)	Allan	Duperow	Seward	683	-18.6	-140.3	44363	27348	27
Jensen et al. (2006)	Allan	Duperow	Seward	683	-18.6	-140.4	43532	27459	24
Wittrup and Kyser (1990)	Allan	Duperow	Seward	683	-18	-139	33800	24200	207
This study	Allan	Duperow	Seward	685	-17.1	-132.2	62200	34200	64.7
Jensen et al. (2006)	Allan	Duperow	Seward	698	-11.7	-120.7	113177	66035	50
Wittrup and Kyser (1990)	Allan	Duperow	Seward	701	-18.1	-138	40900	25700	208
Wittrup and Kyser (1990)	Allan	Duperow	Seward	707	-18.3	-139	42700	24900	211
Wittrup and Kyser (1990)	Allan	Duperow	Seward	713	-17.6	-140	44500	27000	211
Wittrup and Kyser (1990)	Allan	Duperow	Seward	726	-16.9	-137	65900	39300	323
Jensen et al. (2006)	Allan	Duperow	Duperow	734	-17.6	-137	62219	38283	39
Jensen et al. (2006)	Allan	Duperow	Duperow	747	-18.1	-140	61739	36858	37
Jensen et al. (2006)	Allan	Duperow	Duperow	772	-18	-140.3	63816	38493	410
Wittrup and Kyser (1990)	Allan	Duperow	Duperow	774	-18	-138		46600	318
Jensen et al. (2006)	Allan	Duperow	Duperow	786	-14.5	-122.6	47510	24280	112
Jensen et al. (2006)	Allan	Souris River	Souris	813	-10.6	-103	139802	56956	696
Wittrup and Kyser (1990)	Allan	Souris River	Souris	823	-14.9	-124	180000	120000	1810
This study	Allan	Souris River	Souris	823	-16	-125	202000	117000	321
This study	Allan	Souris River	Souris	824	-15.3	-110.7	233000	116000	292
This study	Allan	Souris River	Souris	839	-15.1	-121.7	193000	109000	342
This study	Allan	Souris River	Souris	839	-17.2	-119.2	204000	108000	308
Wittrup and Kyser (1990)	Allan	Souris River	Souris	841	-10.4	-105	136000	73000	1170
Jensen et al. (2006)	Allan	Souris River	Souris	843	-14.9	-123.3	184797	107056	359
Jensen et al. (2006)	Allan	Souris River	Souris	847	-15.2	-124.8	192092	111132	337
Jensen et al. (2006)	Allan	Souris River	Souris	850	-14.6	-123.6	190769	111667	348
Nutrien internal database	Allan	Souris River	Souris	854	-15	-125.3	201924	118552	
Wittrup and Kyser (1990)	Allan	Souris River	Souris	860	-15.1	-125	196000	173000	2030

Jensen et al. (2006)	Allan	Souris River	Souris	899	-14.4	-126	195319	109579	422
Jensen et al. (2006)	Allan	Souris River	Souris	943	-0.5	-47	296602	9844	5050
Jensen et al. (2006)	Allan	Souris River	Souris	952	-3.9	-105.7	348725	4598	6520
Jensen et al. (2006)	Cory	Glacial till		58	-19.7	-154	305	1111	2
Wittrup and Kyser (1990)	Cory	Glacial till		61	-18.8	-150	709	1520	9
Nutrien internal database	Cory	Glacial till		73	-19.3	-144	1067	1080	4
Jensen et al. (2006)	Cory	Cret. Shales		103	-19	-149.2	2764	1902	13
Nutrien internal database	Cory	Cret. Shales		378	-16.5	-129	14790	4907	91
Nutrien internal database	Cory	Cret. Shales		378	-16	-129	7800	5240	77
Jensen et al. (2006)	Cory	Cret. Shales		399	-16	-125.9	15542	8857	28
Wittrup and Kyser (1990)	Cory	Three Forks		524	-15.5	-129		20720	200
Wittrup and Kyser (1990)	Cory	Three Forks		524	-16	-128	28500	19500	160
Wittrup and Kyser (1990)	Cory	Birdbear		593	-13.5	-115	35600	28000	196
Nutrien internal database	Cory	Birdbear		594	-16.8	-135			
Nutrien internal database	Cory	Birdbear		600	-14.4	-122	32000	17300	162
Jensen et al. (2006)	Cory	Birdbear		602	-17.2	-134.9	24916	15996	18
Jensen et al. (2006)	Cory	Birdbear		603	-17.4	-132.5	24819	14990	17
Nutrien internal database	Cory	Birdbear		610	-12.8	-116	33800	2100	186
This study	Cory	Duperow	Seward	623	-14.4	-121.6	29600	17300	67
Wittrup and Kyser (1990)	Cory	Duperow	Seward	626	-16.8	-143	29200	17000	155
Wittrup and Kyser (1990)	Cory	Duperow	Seward	627	-16	-127	29600	17000	129
Jensen et al. (2006)	Cory	Duperow	Seward	635	-16.2	-130.5	16845	16845	20
Wittrup and Kyser (1990)	Cory	Souris River	Souris	647	-9.6	-120	96400	3600	906
Jensen et al. (2006)	Cory	Duperow	Seward	648	-17.4	-135.6	25213	15520	20
Nutrien internal database	Cory	Duperow	Seward	649	-10.4	-136	27890	9396	9
Wittrup and Kyser (1990)	Cory	Duperow	Seward	663	-16.8	-136			
Jensen et al. (2006)	Cory	Duperow	Seward	667	-17.3	-133.8	26803	16757	21
Wittrup and Kyser (1990)	Cory	Duperow	Seward	673	-17	-134	24900	18000	168
Nutrien internal database	Cory	Duperow	Seward	674	-16.5	-133	33800	18300	173
Jensen et al. (2006)	Cory	Duperow	Duperow	692	-17.3	-134.3	27458	16940	22
This study	Cory	Duperow	Duperow	701	-17.3	-131.3	32700	16100	21
Jensen et al. (2006)	Cory	Duperow	Duperow	701	-17.4	-135.8	28584	17250	22
Nutrien internal database	Cory	Souris River	Souris	704	-17.2	-137	30490	12707	11
This study	Cory	Duperow	Duperow	705	-16.9	-132.1	29200	16800	100
This study	Cory	Duperow	Duperow	706	-18.4	-135.6	31400	16100	23
This study	Cory	Duperow	Duperow	707	-16.6	-129.6	30900	17800	22
Jensen et al. (2006)	Cory	Duperow	Duperow	707	-17.3	-135.1	28348	16980	24
Jensen et al. (2006)	Cory	Duperow	Duperow	708	-17.6	-135.5	26874	16875	21
Jensen et al. (2006)	Cory	Souris River	Souris	801	-6	-93.2	153325	51474	995
Nutrien internal database	Cory	Souris River	Souris	827	-9.7	-102	103260	23039	245
This study	Cory	Souris River	Souris	833	-11	-106.9	116000		746
Nutrien internal database	Cory	Souris River	Souris	833	-15.8	-110	98170	21919	205
Jensen et al. (2006)	Cory	Souris River	Souris	837	-10.1	-99.8	110998	34890	691
Nutrien internal database	Cory	Souris River	Souris	847	-9.6	-120	96400	36000	906
Wittrup and Kyser (1990)	Cory	Souris River	Souris	847	-11.2	-103	101000	42000	863
Jensen et al. (2006)	Cory	Souris River	Souris	863	-11.6	-107.1	140537	53624	803
Nutrien internal database	Cory	Souris River	Souris	866	-8.3	-106	160000	103500	1720
Wittrup and Kyser (1990)	Cory	Souris River	Souris	866	-8.3	-106	160000	103500	1720
Nutrien internal database	Cory	Souris River	Souris	872	-11.8	-113	131870	32227	333
Jensen et al. (2006)	Cory	Souris River	Souris	877	-10.1	-98.6	183311	86260	873
Nutrien internal database	Cory	Souris River	Souris	877	-10.4	-103	157060	43280	294
This study	Cory	Souris River	Souris	880	-10.6	-102.9	200000	92500	818
Jensen et al. (2006)	Cory	Souris River	Souris	882	-11.4	-105	167620	75078	754

Nutrien internal database	Cory	Souris River	Souris	890	-10.8	-112	171000	81000	2157
Nutrien internal database	Cory	Souris River	Souris	900	-9.9	-107	194000	173000	2804
Wittrup and Kyser (1990)	Cory	Souris River	Souris	900	-9.6	-107	199000	130000	2800
Nutrien internal database	Cory	Souris River	Souris	908	-8.4	-100	203150	22565	1366
Nutrien internal database	Cory	Souris River	Souris	914	-11.6	-108			
This study	Cory	Souris River	Souris	916	-12	-97.1	224000	52500	2660
This study	Cory	Souris River	Souris	916	-9	-105	192000	46000	2390
This study	Cory	Souris River	Souris	916			235000	44000	2800
This study	Cory	Souris River	Souris	916	-14.1	-105.1	210000	43800	2350
Jensen et al. (2006)	Cory	Souris River	Souris	920	-7.4	-94	207984	52233	2390
Nutrien internal database	Cory	Souris River	Souris	930	-9.2	-102	207000	51000	2206
Wittrup and Kyser (1990)	Cory	Souris River	Souris	930	-8.4	-94	228000	60000	5950
Nutrien internal database	Cory	Dawson Bay		976	-3.6	-67	355000	54870	2174
Jensen et al. (2006)	Cory	Dawson Bay		991	1.8	-53	310760	6986	5400
Jensen et al. (2006)	Cory	Dawson Bay		995	0.6	-48.3	318746	6947	5490
This study	Cory	Dawson Bay		1002	-10.3	-106.6	431000	2300	8200
Nutrien internal database	Cory	Dawson Bay		1006	-1.3	-65			
Jensen et al. (2006)	Rocanville	Lodgepole Fm.		475	-15.7	-125.7	19384	13514	21
Wittrup and Kyser (1990)	Rocanville	Lodgepole Fm.		486	-12.9	-125	19600	13300	119
Wittrup and Kyser (1990)	Rocanville	Lodgepole Fm.		486	-15.6	-121	64715	11970	88
Wittrup and Kyser (1990)	Rocanville	Lodgepole Fm.		486	-17	-138	20400	16000	64
Wittrup and Kyser (1990)	Rocanville	Lodgepole Fm.		500	-14.9	-142	21300	14600	125
Wittrup and Kyser (1990)	Rocanville	Three Forks Gr.		524	-14.9	-111	21000	15600	110
Jensen et al. (2006)	Rocanville	Three Forks Gr.		525	-15.2	-121.6	20116	14603	25
Jensen et al. (2006)	Rocanville	Birdbear		560	-15.2	-119.9	23480	16918	26
Jensen et al. (2006)	Rocanville	Birdbear		562	-14.8	-115.9	30441	21908	38
Wittrup and Kyser (1990)	Rocanville	Birdbear		572	-13.8	-121	28500	21700	154
Wittrup and Kyser (1990)	Rocanville	Birdbear		572	-14.6	-122	29600	24700	108
Nutrien internal database	Rocanville	Duperow	Seward	604	-6.7	-83	120800	105000	500
Wittrup and Kyser (1990)	Rocanville	Duperow	Seward	604	-4.6	-74	110000	79900	647
Wittrup and Kyser (1990)	Rocanville	Duperow	Seward	604	-6	-81	182000	138000	840
Jensen et al. (2006)	Rocanville	Duperow	Seward	610	-5	-65.4	108179	78475	130
Wittrup and Kyser (1990)	Rocanville	Duperow	Seward	610	-4.2	-82	110000	76400	673
Jensen et al. (2006)	Rocanville	Duperow	Seward	625	-5.3	-65.3	107206	76085	136
Jensen et al. (2006)	Rocanville	Duperow	Seward	625	-5.8	-64.3	107764	76584	134
Wittrup and Kyser (1990)	Rocanville	Duperow	Seward	625	-5.1	-81	138700	97000	880
Wittrup and Kyser (1990)	Rocanville	Duperow	Seward	625	-5	-70	81400	52400	510
Nutrien internal database	Rocanville	Duperow	Duperow	672	-6.7	-83	120800	105000	500
Wittrup and Kyser (1990)	Rocanville	Duperow	Duperow	672	-6.7	-83	120800	105000	500
Nutrien internal database	Rocanville	Duperow	Duperow	673	-6	-81	182000	138000	840
Wittrup and Kyser (1990)	Rocanville	Duperow	Duperow	680	-6.2	-82	139000	90000	828
Wittrup and Kyser (1990)	Rocanville	Duperow	Duperow	680	-6.4	-84	142400	69700	720
Jensen et al. (2006)	Rocanville	Duperow	Duperow	688	-7	-73.4	129236	77199	153
Wittrup and Kyser (1990)	Rocanville	Duperow	Duperow	692	-5.5	-82	153500	93000	906
Jensen et al. (2006)	Rocanville	Duperow	Duperow	693	-6.5	-75	125647	74851	148
Wittrup and Kyser (1990)	Rocanville	Duperow	Duperow	695	-6.5	-85	148000	193000	780
Jensen et al. (2006)	Rocanville	Duperow	Duperow	706	-7.1	-73	136019	83187	152
Jensen et al. (2006)	Rocanville	Duperow	Duperow	737	-6.7	-71.3	133343	78930	156
Jensen et al. (2006)	Rocanville	Duperow	Duperow	741	-6.1	-69.6	136196	82190	157
Jensen et al. (2006)	Rocanville	Duperow	Duperow	743	-7.2	-75.3	133061	79230	147

Wittrup and Kyser (1990)	Rocanville	Duperow	Seward	744	-5.9	-86	130000	84000	992
Jensen et al. (2006)	Rocanville	Souris River	Souris	771	-7	-72.8	131987	77271	163
Wittrup and Kyser (1990)	Rocanville	Souris River	Souris	774	-6.6	-84	144900	102000	750
Wittrup and Kyser (1990)	Rocanville	Souris River	Souris	777	-5.5	-80	136000	130000	880
Wittrup and Kyser (1990)	Rocanville	Souris River	Souris	777	-6.4	-74	142400	72100	720
This study	Rocanville	Duperow	Duperow	780	-3.6	-70.3	165000	92900	356
Jensen et al. (2006)	Rocanville	Souris River	Souris	792	-2.9	-58.6	140646	77243	185
Wittrup and Kyser (1990)	Rocanville	Souris River	Souris	792	-1.9	-74	157000	99000	1120
Jensen et al. (2006)	Rocanville	Dawson Bay		878	-2.3	-46.3	187092	111345	267
Jensen et al. (2006)	Rocanville	Dawson Bay		878	-2.4	-45.1	190709	113057	259
Wittrup and Kyser (1990)	Rocanville	Dawson Bay		878	-2.1	-68	186000	118000	2110
Jensen et al. (2006)	Rocanville	Dawson Bay		884	-2.9	-50.4	186902	111553	261
Wittrup and Kyser (1990)	Rocanville	Dawson Bay		884	-1.4	-60	227000	135000	2160
Wittrup and Kyser (1990)	Rocanville	Dawson Bay		884	-1.9	-49	201500	108000	1190
Wittrup and Kyser (1990)	Rocanville	Dawson Bay		887	-1.9	-66	200600	150000	2000
Wittrup and Kyser (1990)	Rocanville	Dawson Bay		890	-1.4	-59	199000	143000	2200
This study	Vanscoy	Cret. Shales		396	-15	-122.8	197000	91500	702
This study	Vanscoy	Duperow	Seward	625	-18.7	-136	44400	24400	21
This study	Vanscoy	Souris River	Souris	796	-18.7	-135.2	53200	36000	42
This study	Vanscoy	Souris River	Souris	929	-17.8	-128.9	52500	32400	40
This study	Vanscoy	Souris River	Souris	941	-14.7	-105.3	311000	77900	1550
This study	Vanscoy	Souris River	Souris	946	-3.4	-61.6	351000	6400	5570
This study	Vanscoy	Souris River	Souris	961	-15.2	-108.6	232000	76700	1240

Table A2: Model setup parameters.

	Depth (m BG)*					
Stratigraphy	**Cory**	**Vanscoy**	**Allan**	**Rocanville**	**n**	**De****
Glacial Till	0	0	0	0	0.24	2.3E-10
Shales	11	11	11	11	0.33	2.3E-10
Mannville	485	485	485	375	0.34	2.3E-10
Three Forks	550	550	560	490	0.1	1.32E-10
Birdbear	590	590	635	530	0.15	9E-10
Seward	625	625	680	550	0.1	1.32E-10
Duperow	675	675	730	625	0.15	9E-10
Souris River	800	800	785	700	0.1	1.32E-10
Manitoba	910	910	875	775	0.15	9E-10
Evaporite	1025	1025	1100	950	0.33	0

*Depths from Marsh and Love (2014).

**De = 1.32E-10 for Three Forks to Manitoba in initial profile.

APPENDIX B

Table B1-1: PCA Plots Fig 3-1a

PCA Report: Transform None, Scaling true (15 rows)

Summary	Count
PCA Report: Transform None, Scaling true (15 rows)	

Summary	Count
Rows	15
Columns	13

	87/86Sr	81Br	d18O	Cl/Br_LO	Cl_ppm_	Na_ppm_	K_ppm_L	Ca_ppm_	Mg_ppm_	Br_ppm_	SO4_ppn	Sr_ppm_LOG
37Cl	1	0.03208	0.7092	-0.1224	0.5955	-0.2843	0.4313	-0.5761	-0.462	-0.4004	-0.4925	0.4441	-0.4421
87/86Sr	0.03208	1	-0.2123	-0.5453	0.45	-0.8541	-0.4104	-0.5073	-0.6435	-0.6949	-0.7085	0.6094	-0.6491
81Br	0.7092	-0.2123	1	0.4957	0.1678	0.06798	0.2228	-0.2709	-0.0907	0.00512	-0.0609	0.08357	-0.0351
d18O	-0.1224	-0.5453	0.4957	1	-0.5928	0.6732	-0.108	0.5957	0.6331	0.7115	0.6955	-0.6568	0.6935
Cl/Br_LOG	0.5955	0.45	0.1678	-0.5928	1	-0.6463	0.4348	-0.7759	-0.8773	-0.8704	-0.9159	0.8361	-0.8755
Cl_ppm_LOG	-0.2843	-0.8541	0.06798	0.6732	-0.6463	1	0.01811	0.8015	0.8602	0.862	0.8982	-0.8669	0.8787
Na_ppm_LOG	0.4313	-0.4104	0.2228	-0.108	0.4348	0.01811	1	-0.2453	-0.3344	-0.2516	-0.2409	0.2995	-0.3391
K_ppm_LOG	-0.5761	-0.5073	-0.2709	0.5957	-0.7759	0.8015	-0.2453	1	0.8641	0.8532	0.8685	-0.8904	0.8758
Ca_ppm_LOG	-0.462	-0.6435	-0.0907	0.6331	-0.8773	0.8602	-0.3344	0.8641	1	0.9824	0.9578	-0.9744	0.9949
Mg_ppm_LOG	-0.4004	-0.6949	0.00512	0.7115	-0.8704	0.862	-0.2516	0.8532	0.9824	1	0.9547	-0.9593	0.9861
Br_ppm_LOG	-0.4925	-0.7085	-0.0609	0.6955	-0.9159	0.8982	-0.2409	0.8685	0.9578	0.9547	1	-0.9375	0.9664
SO4_ppm_LOG	0.4441	0.6094	0.08357	-0.6568	0.8361	-0.8669	0.2995	-0.8904	-0.9744	-0.9593	-0.9375	1	-0.9782
Sr_ppm_LOG	-0.4421	-0.6491	-0.0351	0.6935	-0.8755	0.8787	-0.3391	0.8758	0.9949	0.9861	0.9664	-0.9782	1

Scaled Coordinates	PC1	PC2
37Cl	0.5011	0.7323
87/86Sr	0.6828	-0.5532
81Br	0.06734	0.8429
d18O	-0.7193	0.4146
Cl/Br_LOG	0.8926	0.2234
Cl_ppm_LOG	-0.8989	0.2756
Na_ppm_LOG	0.2729	0.6394
K_ppm_LOG	-0.9049	-0.1648
Ca_ppm_LOG	-0.98	-0.03904
Mg_ppm_LOG	-0.979	0.06815
Br_ppm_LOG	-0.9869	0.0163
SO4_ppm_LOG	0.9693	0.02262
Sr_ppm_LOG	-0.989	5.32E-04

Table B1-2: PCA Plots Fig 3-1b

PCA Report: Transform None, Scaling true (60 rows)

Summary	Count
PCA Report: Transform None, Scaling true (60 rows)	

Summary	Count
Rows	60
Columns	10

Correlation	d18O	Cl/Br_LOG	Cl_ppm_L	Na_ppm_	K_ppm_L	Ca_ppm_	Mg_ppm_	Br_ppm_L	SO4_ppm	Sr_ppm_LOG
d18O	1	-0.8271	0.6679	-0.1608	0.6332	0.8129	0.8117	0.8094	-0.732	0.8406
Cl/Br_LOG	-0.8271	1	-0.7462	0.07167	-0.6671	-0.9164	-0.9078	-0.9497	0.8811	-0.9266
Cl_ppm_LOG	0.6679	-0.7462	1	0.3514	0.7718	0.8699	0.8607	0.9171	-0.8429	0.8661
Na_ppm_LOG	-0.1608	0.07167	0.3514	1	-0.02045	-0.01708	0.013	0.1224	-0.05561	-0.04832
K_ppm_LOG	0.6332	-0.6671	0.7718	-0.02045	1	0.8037	0.7682	0.7625	-0.7176	0.7859
Ca_ppm_LOG	0.8129	-0.9164	0.8699	-0.01708	0.8037	1	0.9763	0.9578	-0.9246	0.9906
Mg_ppm_LOG	0.8117	-0.9078	0.8607	0.013	0.7682	0.9763	1	0.9484	-0.8779	0.9683
Br_ppm_LOG	0.8094	-0.9497	0.9171	0.1224	0.7625	0.9578	0.9484	1	-0.924	0.9622
SO4_ppm_LOG	-0.732	0.8811	-0.8429	-0.05561	-0.7176	-0.9246	-0.8779	-0.924	1	-0.9401
Sr_ppm_LOG	0.8406	-0.9266	0.8661	-0.04832	0.7859	0.9906	0.9683	0.9622	-0.9401	1

Scaled Coordinates	PC1	PC2
d18O	0.8491	-0.248
Cl/Br_LOG	-0.9353	0.1298
Cl_ppm_LOG	0.9017	0.3574
Na_ppm_LOG	0.03182	0.9855
K_ppm_LOG	0.8201	-0.01026
Ca_ppm_LOG	9.86E-01	-0.0432
Mg_ppm_LOG	9.71E-01	-0.01996
Br_ppm_LOG	9.84E-01	0.09043
SO4_ppm_LOG	-9.38E-01	-0.03742
Sr_ppm_LOG	9.89E-01	-0.07612

Title: Hydrogeochemical evolution of groundwaters in the Williston Basin, Canada
Appendix: B

Table B2: Compilation of data.

Source	ID	Mine	Depth	Cl	Na	K	Ca	Mg	Br	SO^4	Sr	B	Fe	Li	Mn	Na/Cl	Cl/Br	δ^{18}O	δ^{2}H	δ^{18}Ocorrected	δ^{2}Hcorrected	^{87}Sr/^{86}Sr	^{87}Sr/^{86}Sr Stf	δ^{37}Cl	δ^{37}Cl Stdv	δ^{81}Br	δ^{81}Br Stdv
			m BG	mg L^{-1}	mg L^{-1}	mg L^{-1}	mg L^{-1}	mg L^{-1}	mg L^{-1}	mg L^{-1}	mg L^{-1}	mg L^{-1}	mg L^{-1}	mg L^{-1}	mg L^{-1}	molar	molar	‰ VSMOW	‰ VSMOW	‰ VSMOW	‰ VSMOW	SRM 987	Stdv ±2se	‰ SMOC	Stdv ±0.1‰	‰ SMOB	Stdv ±0.1‰
Original data	AS16-01	Allan	76	3460	2170	10	62	11	15.4	<2	1.4	1.9	<0.005	0.27	0.008	0.967200574	506.373428	-17.37947135	-135.7153608	-17.40663158	-135.7585354			0.100071894	0.085040635	1.648524121	0.026646376
Original data	AS18-01	Allan	76	3700	2170	8	57	9.9	100	0.5	1.5	2	0.1	0.28	<0.05	0.904463239	83.39062985	-18.56681809	-134.6797162	-18.59399164	-134.7219732			0.352162037	0.075731123		
Original data	VPO-1300VBT	Vanscoy	396	197000	91500	4150	14400	4300	702	630	328	33	0.1	9	0.27	0.71628817	632.4768646	-14.21773348	-119.3395925	-15.00246372	-122.8395275	0.708365	0.000009	-0.154901522	0.083639256	0.680437501	0.109848591
Original data	23981	Lanigan	490	29900	17600	200	1080	370	138	4000	30	5	0.14	1.9	0.73	0.907766998	488.3235081										
Original data	CS16-07	Cory	623	29600	17300	1020	1650	700	67.3	4900	34	3	<0.05	3	0.13	0.901337214	991.2704885	-14.20459948	-120.9813183	-14.39000218	-121.6258331	0.708808	0.000014	-0.13578389	0.098079808	0.51972439	0.08970012
Original data	VS18-01	Vanscoy	625	44400	24400	1300	2000	700	20.6	5100	38	2	<0.05	2.8	0.15	0.847500117	4857.706593	-18.4	-135.2	-18.66788797	-135.9829325			0.241183978	0.08809444	0.487254465	0.099888343
Original data	AS16-02	Allan	669	50200	28200	2130	1900	710	174	5000	38	4	<0.05	1.7	<0.05	0.866319922	650.2344856	-17.19774981	-134.1295367	-17.51229977	-134.9925487	0.708653	0.000012	-0.098717973	0.049059646	0.297679086	0.038007243
Original data	AS18-02	Allan	669	47800	27800	2200	1800	690	18.4	5500	37	3	0.06	1.7	<0.05	0.896911949	5854.98253	-18.4282269	-134.6842027	-18.73929431	-135.5300571			0.00135466	0.114834769	0.438665308	0.11480005
Original data	AS16-03	Allan	672	45100	26900	2100	1800	660	90	5200	39	2	0.28	1.7	0.12	0.919832285	1129.404626	-16.81353722	-133.4416764	-17.11597783	-134.2681896	0.70864	0.000009	0.021082119	0.101144578	0.573450362	0.108385821
Original data	AS18-03	Allan	672	47500	28800	2300	2000	770	17.8	6400	36	3	<0.05	1.6	<0.05	0.935043442	6014.356085	-17.85512517	-135.4645178	-18.17468576	-136.3659186			0.133133156	0.110253028	0.63525617	0.087969629
Original data	AS16-04	Allan	685	62200	34200	2520	2100	780	64.7	5000	43	3	<0.05	1.9	<0.05	0.847946851	2166.714222	-16.74737161	-131.2038563	-17.12744436	-132.1983792	0.708662	0.00001	0.078614818	0.036442444	0.463073717	0.078143471
Original data	23982	Lanigan	694	35200	20000	1460	1470	490	56	5500	30	2	1.4	2.1	0.43	0.876234286	1416.674793										
Original data	SC LAN OBS2 WELL SWAB 032620	Lanigan	694	176000	91100	2010	4100	1610	223	1700	91	18	2890	9.2	21	0.798249435	1778.784493	-15.14736801	-121.9502056	-16.05467308	-123.8839666			0.152499583	0.072163546	0.595046868	0.056658945
Original data	CS18-04	Cory	701	32700	16100	1050	1580	810	20.8	5000	36	4	1.4	2.9	<0.05	0.759295863	3543.234922	-17.16031522	-130.670869	-17.32593809	-131.3017699			0.341645479	0.105066032	0.615640331	0.077680105
Original data	CS16-05	Cory	705	29200	16800	980	1510	780	100	4700	34	4	<0.05	2.6	<0.05	0.887277239	658.1098356	-16.70168413	-131.4758792	-16.87757247	-132.1000745	0.708721	0.00001	0.075889325	0.090779627	0.522313706	0.083654704
Original data	CS18-03	Cory	706	31400	16100	980	1450	720	23.4	4600	35	4	<0.05	2.9	<0.05	0.790731679	3024.330997	-18.26718719	-134.98736	-18.43653538	-135.5801942			0.196508839	0.095683499	0.536651484	0.048775123
Original data	CS16-08	Cory	707	30900	17800	1050	1670	850	21.9	4800	35	3	<0.05	2.6	<0.05	0.888371123	3180.020316	-16.41172853	-128.9502817	-16.59666186	-129.6257875	0.708712	0.00001	0.206041484	0.053375508	0.617242082	0.351806326
Original data	SC16-01	Rocanville	780	165000	92900	2120	2690	1980	356	3200	100	100	<0.05	38.3	0.17	0.868289762	1044.598688	-2.662282657	-68.29788327	-3.595894735	-70.28484878	0.708112	0.000011	0.199821168	0.070676407	1.06875	0.088549825
Original data	JANS-PS-785	Jansen	785	101000	52300	870	2790	1310	132	3700	65	34	0.23	9.2	<0.05	0.798570431	1724.499102	-16.89070364	-123.2224765	-17.43766561	-124.5247377			0.002960873	0.107151687	0.536882737	0.084489906
Original data	VS18-02	Vanscoy	796	53200	36000	1500	2400	860	42.4	4900	48	2	<0.05	3.2	<0.05	1.04357527	2827.882144	-18.3	-134.2154391	-18.69618417	-135.2371449			0.061712119	0.109505378	0.849619733	0.073739027
Original data	BHPB-JANSEN	Jansen	806	134000	69000	1150	5000	1890	253	1900	118	36	5.2	12.5	0.12	0.794103669	1193.71268	-14.78206191	-120.5044195	-15.47122812	-122.345333			0.406131838	0.099521199	0.45473776	0.038221562
Original data	23983	Lanigan	821	177000	95900	5350	3970	1640	220	2100	90	11	8.1	7.3	1.2	0.835561174	1813.285194										
Original data	SC LAN OBS4 WELL SWAB 032620	Lanigan	821	105000	46300	12400	2560	1430	82.5	4200	42	16	492	7.6	5.3	0.680024567	2868.473754	-16.72715879	-121.5264947	-17.23160439	-123.284608			0.19484738	0.089912513	0.156579897	0.0810554
Original data	AS16-05	Allan	823	202000	117000	2290	5660	1940	321	950	126	20	0.16	9.7	<0.05	0.893238437	1418.279635	-14.8696271	-122.6395276	-15.99501926	-125.0404646	0.708128	0.000008	0.038124473	0.08161809	0.543257625	0.092042116
Original data	AS18-05	Allan	824	233000	116000	2200	5600	1900	292	970	129	22	0.24	9.7	0.06	0.767776789	1798.409548	-14.25269369	-108.2928676	-15.34684862	-110.654903			-0.12802464	0.121113525	0.626763215	0.012867078
Original data	CS16-04	Cory	833	116000	34700	1510	20900	6790	746	800	410	70	<0.05	27.3	0.11	0.461322244	350.4569619	-10.94084977	-102.6669958	-11.04365559	-106.8604173	0.708184	0.00001	0.219047944	0.07647266	0.967976468	0.094566231
Original data	AS16-06	Allan	839	193000	109000	2600	6600	2200	342	1000	140	20	0.53	10.6	0.14	0.8709678	1271.881742	-14.04305491	-119.2294592	-15.08950681	-121.7214119	0.708153	0.00001	0.032131622	0.101110339	0.513217127	0.092991384
Original data	AS18-06	Allan	839	204000	108000	2400	6200	2100	308	890	130	20	1.6	9	0.12	0.816444182	1492.777158	-16.18698818	-116.7752589	-17.21729609	-119.1783029			0.04899062	0.090287557	0.42028973	0.114428977
Original data	CS16-03	Cory	880	200000	92500	2950	18400	3890	818	420	360	60	1	14.3	0.14	0.713254709	551.051542	-9.818307904	-98.97015744	-10.61631732	-102.8728857	0.708061	0.000012	0.124915586	0.094618274	0.6625	0.098107084
Original data	CS16-01	Cory	916	224000	52500	10300	51800	14000	2660	160	1150	100	0.11	21.5	0.7	0.361446643	189.7937521	-12.04394222	-88.27464706	-12.04146415	-97.09071433	0.708101	0.000012	-0.014099612	0.088667147	0.394866214	0.069042698
Original data	CS16-02	Cory	916	192000	46000	9300	46200	13400	2390	240	940	90	0.42	20	0.47	0.369478791	181.0584748	-9.042011851	-96.78989041	-9.000455655	-104.9659501	0.708101	0.000012	-0.322907665	0.095545544	0.316405407	0.066872953
Original data	CS18-01	Cory	916	235000	44000	9780	50100	13200	2800	180	1280	110	3.6	25	0.7	0.288747162	189.158282							-0.235610562	0.090922761	0.235544692	0.04572997
Original data	CS18-02	Cory	916	210000	43800	8670	41600	12100	2350	250	960	88	11	22.4	0.53	0.321653089	201.4034763	-14.16101915	-97.78564361	-14.14821825	-105.1420512			-0.0792797	0.108136374	0.306060316	0.024511022
Original data	VS18-03	Vanscoy	929	52500	32400	1400	2000	920	40	4800	50	3	<0.05	4.3	0.09	0.951740646	2958.113559	-17.4	-128.0091277	-17.75292569	-128.946025			0.341700262	0.105368638	0.519254919	0.088486315
Original data	VS18-04	Vanscoy	941	311000	77900	5900	28200	6900	1550	280	870	92	0.45	21.1	0.31	0.386286899	452.2142264	-14.2	-100.3267296	-14.69224495	-105.3019221			0.047137315	0.117771931	0.674038192	0.023738679
Original data	VPO-3105-06	Vanscoy	946	351000	6400	18000	129000	22200	5570	26	4000	90	3.8	16.6	16	0.028119382	142.0258677	-4.132301094	-44.65303576	-3.358494726	-61.57045516	0.708439	0.00001	-0.096053008	0.067403343	0.685	0.070474582
Original data	VS18-05	Vanscoy	961	232000	76700	5900	28200	6800	1240	260	700	96	0.21	12.1	0.37	0.509847495	421.6788606	-14.7	-103.3541127	-15.21101175	-108.5636666			-0.105217253	0.088970962	0.218445144	0.085306218
Original data	SC16-02	Rocanville	1000	125000	69600	1760	3290	1900	206	3600	93	70	<0.05	25.1	0.08	0.858681561	1367.597577	-5.993760509	-81.92200555	-6.704780679	-83.68714888	0.708114	0.000011	0.206439677	0.059405983	0.912857143	0.091234914
Original data	CS16-09	Cory	1002	431000	2300	8100	182000	19400	8200	85	4350	200	5.2	46.8	16	0.00822969	118.4619692	-11.07629929	-87.68021193	-10.30176757	-106.613872	0.70818	0.000005	-0.24243814	0.081236785	0.388495392	0.069253103
Original data	CM16-01	Cory	1012	277000	18400	20000	94700	17700	3820	52	2820	60	9.8	10.9	8.2	0.102440329	163.4300585	-7.636584412	-62.34627751	-7.135672302	-76.04541685	0.708964	0.000011	0.033763183	0.11214389	0.7775	0.035939764
Original data	CM16-02	Cory	1012	338000	6100	22200	125000	21400	5400	31	4140	80	24	16.8	18	0.027832104	141.0712357	-5.075172907	-46.2778436	-4.332352085	-62.97680925	0.708377	0.000012	-0.035011012	0.101951079	0.795	0.02081666
Original data	CM16-03	Cory	1012	361000	6800	27000	131000	23500	5550	25	4290	90	20	18.8	18	0.02904923	146.598575	-4.818441442	-47.23064346	-4.039579089	-64.59469727	0.708435	0.000014	0.042637827	0.066229038	0.86	0.033665016
Original data	CM16-04	Cory	1012	352000	5800	22600	130000	22700	6040	21	4310	80	32	17.5	22	0.025410794	131.3473318	-4.586997638	-48.87918123	-3.805508683	-66.00158399	0.708322	0.000008	-0.223634992	0.08970891	0.90032029	0.110971658
Original data	CM17-01	Cory	1012	320000	14000	18800	99100	17300	4740	42	3380	90	23	16.8	10	0.06747004	152.1553287	-10.0454219	-66.44793788	-9.519897343	-80.00418731			-0.319259675	0.096626602	0.481262765	0.080228477
Original data	CM18-01	Cory	1012	306000	14500	17800	99300	17400	4930	40	3410	90	28	17.3	10	0.073076794	139.8910846	-8.951791818	-63.18690502	-8.419531797	-76.92008152			-0.262250906	0.068739842	0.53675471	0.069545201
Original data	CM18-02	Cory	1012	350000	6230	20100	101000	33200	5780	21	3480	30	75	12.6	29	0.027450668	136.4758274	-8.194858483	-51.12083664	-7.143321388	-66.88955102			-0.144728546	0.097026407	0.320126693	0.029828309
Original data	CM18-03	Cory	1012	362000	5680	20600	128000	22200	6060	24	4340	90	21	19.2	23	0.024197621	134.6329855							-0.086392279	0.092470441	0.690977634	0.046016169
Original data	CM18-04	Cory	1012	362000	6040	21300	125000	22300	5890	23	4230	70	35	14	22	0.025731273	138.5188272							-0.134865257	0.094345315	0.662666519	0.042640013
Original data	CM18-05	Cory	1012	356000	5580	20800	137000	23200	6140	24	4200	90	20	20	18	0.024172252	130.6763986							-0.014300245	0.093608215	0.73718905	0.059043639
Original data	LM17-01	Lanigan	1051	327000	8080	12000	124000	16800	5500	31	5300	40	45	10.3	13	0.038106277	133.9987025	-5.260851406	-36.26589961	-4.639734232	-52.2545722			0.076447975	0.084946717	0.815373982	0.098224684
Original data	VPO-PANEL9	Vanscoy	1098	196000	92800	5620	14000	4350	691	590	324	33	<0.05	8.9	0.28	0.730171395	639.2835863	-14.25105011	-120.6475194	-15.0516359	-124.183984	0.7084	0.00001	0.029931636	0.100815212	0.58375	0.06045955
Original data	VPO-3604-5	Vanscoy	1098	424000	3200	28500	188000	13000	6110	38	6500	150	0.3	37.2	25	0.011639037	156.4012344	-12.21442219	-95.52255051	-11.65903277	-114.602674	0.708623	0.000011	-0.218663073	0.056225809	0.361968273	0.080717929
Original data	VM18-01	Vanscoy	1098	215000	95200	7500	12400	4200	657	550	314	37	0.08	8.5	0.36	0.682859568	737.5451651	-17.1	-123	-17.92347985	-126.3918249			-0.026115471	0.086421776	0.686252382	0.099749605
Original data	VM18-02	Vanscoy	1098	358000	5300	15700	123000	24500	5250	22	4420	68	3.3	18.3	18	0.022831043	153.6877502	-7.6	-49.6	-6.756895433	-66.0399464			0.084318105	0.104854536	0.774436716	0.112275414
Original data	VM18-04	Vanscoy	1098	167000	84200	3800	11200	3900	617	660	296	35	0.34	7.8	0.24	0.777550367	610.0238812	-17	-124	-17.74698072	-127.0604453			0.006345207	0.11927524	0.636304023	0.043026087
Original data	AM18-01	Allan	1105	360000	5600	11400	125000	22100	5600	24	4600	58	4.6	14.7	16	0.023989348	144.8871947	-7.621984611	-51.53992223	-6.836785704	-67.67747522			-0.011432644	0.095921756	0.626844333	0.042320604
Original data	AM18-02	Allan	1105	347000	6000	16200	122000	23200	5380	26	4560	57	0.63	14.5	14	0.026665804	145.3659628	-7.100269454	-44.57528153	-6.297389029	-60.98124038			-0.060408852	0.105285011	0.723482303	0.066969812
Original data	AM18-03	Allan	1105	405000	5200	13000	134000	22700	6120	24	4710	55	15	13.2	17	0.019800731	149.1485828	-8.265772723	-55.4155867	-7.478353029	-71.89712642			0.010151251	0.110499056	0.841279527	0.087473559
Original data	AM16-01	Allan	1105	355000	7400	23200	126000	23800	6040	28	4310	60	0.5	14.1	14	0.032146691	132.4667693	-4.927966842	-42.24066186	-4.138343952	-59.25212347	0.708594	0.00001	-0.109777201	0.081499102	0.670595391	0.054740227
Original data	AM16-02	Allan	1105	336000	7200	12200	131000	23200	5490	28	4500	60	2.9	15	18	0.03304655	137.9375357	-4.75797625	-46.56565938	-3.936428524	-63.7596562	0.708458	0.00001	-0.158340516	0.097305865	0.483368246	0.071709397
Original data	AM17-01	Allan	1105	339000	6270	12100	124000	21900	6110	22	4570	60	<0.5	13.8	18	0.028523365	125.0472133							-0.054894371	0.108963082	0.814277706	0.080320937
Jensen et al. (2006)	3325	Cory	53	305	1111	11	25	6	2	1803	0.381					5.61736	343.70462	-19.7	-154								
Jensen et al. (2006)	2314	Allan	89	3021	2015				14							1.02859	486.33802	-18.3	-140.6								
Jensen et al. (2006)	3344	Cory	94	2764	1902	12	38	7	13	11	0.841					1.06118	479.19273	-19	-149.2								
Jensen et al. (2006)	2315	Allan	94	3181	1959	15	57	8	14	10	1.24					0.94971	512.09574	-18.1	-138.9								
Jensen et al. (2006)	2316	Allan	136	4529	2689	16	99	16	19	9	2.53					0.9156	537.23494	-17.2	-133.2								
Jensen et al. (2006)	2313	Allan	173	3978	2494	12	67	11	17	10	1.62					0.96683	527.38939	-17.4	-135.2								
Jensen et al. (2006)	2317	Allan	263	8784	5396	44	212	61	25	26	6.93					0.94732	791.89545	-15.7	-121.3								
Jensen et al. (2006)	2318	Allan	302	9519	5712	54	227	77	27	26	7.85					0.92537	794.59	-15	-118.5								
Jensen et al. (2006)	2312	Allan	344	12364	7948				53							0.99133	525.77346	-15.6	-120.5								
Jensen et al. (2006)	3326	Cory	363	15542	8857	337	873	196	28	1290	26.1					0.87882	1251.02043	-16	-125.9								
Jensen et al. (2006)	3327	Cory	547	24916	15996	851	1470	495	18	4560	31.3					0.99004	3119.76116	-17.2	-134.9								
Jensen et al. (2006)	3343	Cory	548	24819	14990	898	1430	557	17	4920	28					0.9314	3290.4166	-17.4	-132.5								
Jensen et al. (2006)	2319	Allan	554	37863	22193				23							0.9039	3710.24608	-10.4	-105.7								
Jensen et al. (2006)	3328	Cory	578	16845	16845	1030	1500	650	20	5010	31.9					1.54212	1898.26373	-16.2	-130.5								
Jensen et al. (2006)	3329	Cory	589	25213	15520	1060	1630	695	20	5370	31.3					0.94926	2841.25399	-17.4	-135.6								
Jensen et al. (2006)	3342	Cory	606	26803	16757	456	683	323	21	2268	32.8					0.96412	2876.6011	-17.3	-133.8								
Jensen et al. (2006)	2320	Allan	619	42714	27391	2290	1890	699	24	6000	36.7					0.98891	4011.20199	-18.3	-141.3								
Jensen et al. (2006)	2309	Allan	621	44482	27219	2280	1870	688	28	4770	36.6					0.94364	3580.48455	-18.4	-140.1								
Jensen et al. (2006)	2310	Allan	621	44363	27348	2340	1890	691	27	6060	36.8					0.95066	3703.16167	-18.6	-140.3								
Jensen et al. (2006)	2311	Allan	621	43532	27459	2300	1880	692	24	6150	36.4					0.97273	4088.01903	-18.6	-140.4								
Jensen et al. (2006)	3341	Cory	629	27458	16940	1100	1450	806	22	5220	34					0.9514	2812.9483	-17.3	-134.3								
Jensen et al. (2006)	2308	Allan	635	113177	66035				50							0.89978	5101.56828	-11.7	-120.7								
Jensen et al. (2006)	3330	Cory	637	28584	17250	1070	1540	761	22	5220	33.5					0.93065	2928.30192	-17.4	-135.8								
Jensen et al. (2006)	3331	Cory	643	28348	16980	1060	1500	750	24	5070	33.7					0.92371	2662.11439	-17.3	-135.1								
Jensen et al. (2006)	3340	Cory	644	26874	16875	1080	1480	778	21	5190	33.4					0.96834	2884.22109	-17.6	-135.5								
Jensen et al. (2006)	2307	Allan	667	62219	38283	2730	2140	767	39	5820	40					0.94886	3595.62134	-17.6	-137								
Jensen et al. (2006)	2321	Allan	679	61739	36858	2470	1960	496	37	4710	41.2					0.92064	3760.74076	-18.1	-140								
Jensen et al. (2006)	2306	Allan	702	63816	38493	2960	2210	660	41	5670	41.3					0.93019	3508.01347	-18	-140.3								
Jensen et al. (2006)	2305	Allan	714	47510	24280	580	1830	763	112	1104	88.2					0.7881	956.05425	-14.5	-122.6								
Jensen et al. (2006)	3339	Cory	728	153325	51474	2340	26800	8410	995	519	459					0.51772	347.30051	-6	-93.2								
Jensen et al. (2006)	2304	Allan	739	139802	56956	1740	18500	5640	696	756	353					0.62827	452.70957	-10.6	-103								
Jensen et al. (2006)	3332	Cory	761	110998	34890	1470	20100	6370	691	1122	397					0.48473	362.03673	-10.1	-99.8								
Jensen et al. (2006)	2322	Allan	766	184797	107056	2040	6560	2290	359	1149	138					0.89338	1160.15495	-14.9	-123.3								
Jensen et al. (2006)	2323	Allan	770	192092	111132	2300	6260	2130	337	1089	150					0.89217	1284.67984	-15.2	-124.8								
Jensen et al. (2006)	2324	Allan	773	190769	111667	2360	6510	2160	348	1080	144					0.90268	1235.50381	-14.6	-123.6								
Jensen et al. (2006)	3338	Cory	784	140537	53624	2280	22000	5980	803	828	390					0.58842	394.44882	-11.6	-107.1								
Jensen et al. (2006)	3337	Cory	797	183311	86260	3170	19900	3980	873	606	407					0.72567	473.24912	-10.1	-98.6								
Jensen et al. (2006)	3333	Cory	802	167620	75078	2820	19300	4200	754	654	402					0.69073	501.03726	-11.4	-105								
Jensen et al. (2006)	2303	Allan	817	195319	109579	3240	8790	2790	422	897	191					0.86517	1043.15194	-14.4	-126								
Jensen et al. (2006)	3334	Cory	836	207984	52233	9250	43700	2500	2390	30	1070					0.38729	196.13159	-7.4	-94								
Jensen et al. (2006)	2302	Allan	857	296602	9844	9600	118000	17900	5050	201	4030					0.05118	132.37264	-0.5	-47								
Jensen et al. (2006)	2301	Allan	865	348725	4598				6520							0.02033	120.5455	-3.9	-105.7								
Jensen et al. (2006)	3336	Cory	901	310760	6986	20100	124000	20100	5400	258	3660					0.03467	129.70206	1.8	-53.2								
Jensen et al. (2006)	3335	Cory	905	318746	6947	19200	124000	20200	5490	273	3900					0.03361	130.85428	0.6	-48.3								
Nutrien internal database	CSBR 02-325	Cory	53	304.86585	1110.83996	11	24.8	5.7	2.29							5.61903	300.04669	-19.67015	-153.95776								
Nutrien internal database	CS86-01	Cory	55	709	1520	166	30	7	9	1803						3.3061	177.54942	-18.8	-150								
Nutrien internal database	CS86-02	Cory	66	1067	1080	2	26	13	4		0.42					1.56091	601.20137	-19.3	-144								
Nutrien internal database	ASBR 02-314	Allan	89	3020.83129	2014.58982				14.2							1.02844	479.46141	-18.33802	-140.58384								
Nutrien internal database	CSBR 02-344	Cory	94	2763.72994	1902.26266	12	37.7	7.1	12.6							1.06143	494.35689	-19.01658	-149.18754								
Nutrien internal database	ASBR 02-315	Allan	94	3180.8323	1959.20176	15	56.6	7.6	13.9							0.94985	515.75269	-18.13171	-138.92015								
Nutrien internal database	AS86-01	Allan	111	354	2050	3	73	6	32	9.9						8.93036	24.93267	-17.5	-129								
Nutrien internal database	ASBR 02-316	Allan	136	4528.86047	2689.0407	16	98.6	16	19.1							0.91564	534.40573	-17.20322	-133.18736								
Nutrien internal database	AS86-02	Allan	144	530	2280	6	85	8	32	8.7						6.63403	37.32858	-17	-136								
Nutrien internal database	ASBR 02-313	Allan	166	3978.21909	2493.62377	12	67.3	11	16.9		1.55					0.96663	530.53925	-17.37188	-135.22905								
Nutrien internal database	ASBR 02-317	Allan	263	8784.31075	5395.96514	44	212	61	24.5	9.9						0.94728	808.08517	-15.73995	-121.2623								
Nutrien internal database	ASBR 02-318	Allan	302	9518.97168	5712.04391	54	227	76.9	26.8	26.1						0.92538	800.51739	-14.99524	-118.53145								
Nutrien internal database	AS86-03	Allan	310	1020	6250	45	362	84	76	25.5						9.44927	30.24838	-13.4	-119								
Nutrien internal database	CS86-03	Cory	343	14790	4907	128	771	368	91	10.8						0.51164	366.30455	-16.5	-129								
Nutrien internal database	ASBR 02-312	Allan	344	12363.54387	7948.36876				53.06824		10.16					0.99141	525.07797	-15.5832	-120.47252								

Nutrien internal database	CS86-04	Corv	344	7800	5240	121	58	65	77			1.03599	228.30709	-16	-129
Nutrien internal database	CSBR 02-326	Cory	363	15542.19683	8857.26211	337	873	196	28.4			0.87883	1233.41605	-16.00825	-125.89339
Nutrien internal database	RMBR 02-356	Rocanville	431	19383.63847	13513.72988	239	776	436	21.15		3203.36	1.07512	2065.57258	-15.73014	-125.67037
Nutrien internal database	RS86-02	Rocanville	442	64715	11970	717	1260	488	88		59.44	0.28524	1657.43999	-15.6	-121
Nutrien internal database	RS86-03	Rocanville	442	20400	16000	188	1010	470	64		19.77	1.20951	718.39901	-17	-138
Nutrien internal database	RS86-01	Rocanville	442	19600	13300	238	1177	515	119	5010		1.04644	371.21425	-12.9	-125
Nutrien internal database	RS86-04	Rocanville	455	21300	14600	108	713	411	125			1.05704	384.04766	-14.9	-142
Nutrien internal database	CS86-05	Corv	476		20720	1188	2341	450	200	1290				-15.5	-129
Nutrien internal database	CS86-06	Corv	476	28500	19500	955	1841	470	160			1.05514	401.45827	-16	-128
Nutrien internal database	RS86-05	Rocanville	476	21000	15600	108	1123	3.1	110		17.43	1.14558	430.27106	-14.5	-111
Nutrien internal database	RMBR 02-355	Rocanville	477	20116.09775	14602.89001	214	872	333	24.65			1.11947	1839.25669	-15.18751	-121.62591
Nutrien internal database	RMBR 02-354	Rocanville	509	23479.64601	16918.10294	250	962	348	26.24	6960		1.11116	2016.70904	-15.15178	-119.92916
Nutrien internal database	RMBR 02-365	Rocanville	511	30440.69883	21908.24254	522	716	278	37.55	7590		1.10987	1827.09112	-14.81728	-115.86394
Nutrien internal database	RS86-07	Rocanville	520	29600	24700	272	1090	257	108		14.84	1.28684	617.70837	-14.6	-122
Nutrien internal database	RS86-06	Rocanville	520	28500	21700	161	1248	420	154	18240		1.17418	417.0995	-13.8	-121
Nutrien internal database	CS86-07	Cory	539	35600	28000	1360	1964	870	196			1.2129	409.36382	-13.5	-115
Nutrien internal database	CS86-08	Cory	540											-16.8	-135
Nutrien internal database	CS86-09	Cory	545	32000	17300	1143	1917	760	162			0.83371	445.19522	-14.4	-122
Nutrien internal database	CSBR 02-327	Cory	547	24915.52296	15996.35766	851	1470	495	17.83813			0.99008	3148.01112	-17.23017	-134.86989
Nutrien internal database	CSBR 02-343	Cory	548	24818.90424	14989.85816	898	1430	557	17.19366	4560		0.93139	3253.3427	-17.38153	-132.48588
Nutrien internal database	RS86-09	Rocanville	549	110000	79900	392	2330	313	647		8.71	1.12014	383.18097	-4.6	-74
Nutrien internal database	RS86-08	Rocanville	549	120800	105000	400	632	370	500			1.34042	544.51827	-6.7	-83
Nutrien internal database	RS86-10	Rocanville	549	182000	138000	3750	340	2460	840			1.1693	488.32351	-6	-81
Nutrien internal database	ASBR 02-319	Allan	554	37863.49932	22193.45352				22.9			0.9039	3726.49718	-10.35697	-105.74052
Nutrien internal database	RMBR 02-353	Rocanville	554	108179.4137	78475.15233	590	791	270	129.95			1.11868	1876.22047	-4.9892	-65.44148
Nutrien internal database	RS86-11	Rocanville	554	110000	76400	400	763	301	673	18990		1.07107	368.37755	-4.2	-82
Nutrien internal database	AS86-04	Allan	554	26700	15500	320	1840	100	148			0.89524	406.59785	-18.1	-138
Nutrien internal database	CS86-10	Corv	554	33800	2100	1010	3180	640	186	4920		0.09581	409.56165	-12.8	-116
Nutrien internal database	RMBR 02-363	Rocanville	568	107205.6133	76085.36333	540	736	280	135.98		8.07	1.09447	1776.87967	-5.30984	-65.28765
Nutrien internal database	RMBR 02-364	Rocanville	568	107763.7162	76583.89042	300	1030	406	133.97	18570		1.09593	1812.9279	-5.8311	-64.30417
Nutrien internal database	RS86-12	Rocanville	568	138700	97000	720	1014	350	880	9390		1.07848	355.22974	-5.1	-81
Nutrien internal database	RS86-13	Rocanville	568	81400	52400	410	574	120	510		24.97	0.99272	359.72429	-5	-70
Nutrien internal database	CS86-11	Corv	569	29200	17000	430	1954	820	155			0.89781	424.58699	-16.8	-143
Nutrien internal database	CS86-12	Corv	570	29600	17000	430	2202	670	12945			0.88568	5.15353	-16	-127
Nutrien internal database	CSBR 02-328	Corv	578	16844.71432	16844.71432	1030	1500	650	20.12706			1.54212	1886.24813	-16.20961	-130.50367
Nutrien internal database	CSBR 02-329	Cory	589	25213.1739	15520.06798	1060	1630	695	19.65706	5010		0.94926	2890.84238	-17.35462	-135.6171
Nutrien internal database	CS92-01	Corv	590	27890	9396	680	1064	426	9.1	5370		0.51953	6907.52797	-10.4	-136
Nutrien internal database	AS86-05	Allan	596	31000	19800	1465	2216	330	160		32.05	0.98497	436.67391	-17.6	-136
Nutrien internal database	CS86-13	Corv	603								27.47			-16.8	-136
Nutrien internal database	CSBR 02-342	Corv	606	26803.22495	16757.29853	456	683	323	21.24756			0.96413	2843.10955	-17.33046	-133.75901
Nutrien internal database	RS86-14	Rocanville	611	120800	105000	400	632	370	500			1.34042	544.51827	-6.7	-83
Nutrien internal database	RS86-15	Rocanville	611	182000	138000	3750	340	2460	840			1.1693	488.32351	-6	-81
Nutrien internal database	CS86-14	Cory	612	24900	18000	540	2010	830	168	2268		1.11479	334.04548	-17	-134
Nutrien internal database	CS86-15	Corv	613	33800	18300	630	2183	620	173		20.35	0.83494	440.33796	-16.5	-133
Nutrien internal database	RS86-16	Rocanville	618	142400	69700	3190	3560	710	720		37	0.75482	445.75172	-6.4	-84
Nutrien internal database	RS86-17	Rocanville	618	139000	90000	2160	4040	1170	828		38.07	0.9985	378.35545	-6.2	-82
Nutrien internal database	ASBR 02-320	Allan	619	42713.5693	27391.37691	2290	1890	699	23.7		39.97	0.98893	4061.93574	-18.34814	-141.32144
Nutrien internal database	ASBR 02-309	Allan	621	44481.77381	27218.93593	2280	1870	688	27.89671	6000		0.94364	3593.72345	-18.41145	-140.0773
Nutrien internal database	ASBR 02-310	Allan	621	44362.62345	27348.37266	2340	1890	691	26.68633	5880		0.95068	3746.65731	-18.60101	-140.28619
Nutrien internal database	ASBR 02-311	Allan	621	43532.29412	27459.15026	2300	1880	692	24.47181	6060		0.97273	4009.22964	-18.61508	-140.39926
Nutrien internal database	AS86-06	Allan	621	33800	24200	1240	2098	530	207	6150		1.10412	368.01192	-18	-139
Nutrien internal database	RMBR 02-352	Rocanville	626	129235.5362	77199.37898	3320	3280	1480	153.49			0.92119	1897.65559	-6.98537	-73.35871
Nutrien internal database	CSBR 02-341	Cory	629	27458.24675	16939.87008	1100	1450	806	21.56527			0.95138	2869.68013	-17.27439	-134.30428
Nutrien internal database	RS86-18	Rocanville	629	153500	93000	2450	3920	1250	906	2985		0.93431	381.85256	-5.5	-82
Nutrien internal database	RMBR 02-362	Rocanville	630	125646.5248	74850.50171	3260	3470	1230	147.98		40.33	0.91868	1913.65211	-6.5	-75
Nutrien internal database	RS83-01	Rocanville	632	148000	193000	3910	3150	2070	780	3480		2.01101	427.64426	-6.5	-85
Nutrien internal database	ASBR 02-308	Allan	635	113176.9713	66034.55199				49.81954			0.89977	5120.04659	-11.70825	-120.6566
Nutrien internal database	CSBR 02-330	Cory	637	28584.36623	17249.76987	1070	1540	761	21.8		5220	0.93062	2955.20494	-17.42733	-135.83871
Nutrien internal database	AS86-07	Allan	637	40900	25700	1390	2059	520	208			0.96901	443.17525	-18.1	-138
Nutrien internal database	CS92-02	Corv	640	30490	12707	680	1390	610	11.4	5220		0.64269	6027.92865	-17.2	-137
Nutrien internal database	RMBR 02-361	Rocanville	642	136019.2613	83187.03357	3680	3060	1270	152.17			0.94313	2014.59105	-7.0804	-72.95038
Nutrien internal database	AS86-08	Allan	643	42700	24900	1250	2007	330	211		28.91	0.89927	456.10092	-18.3	-139
Nutrien internal database	CSBR 02-331	Cory	643	28348.07335	16980.09682	1060	1500	750	23.96967		22.85	0.92371	2665.49024	-17.26139	-135.1457
Nutrien internal database	CSBR 02-340	Corv	644	26874.36416	16875.44756	1080	1480	778	21.08039	5070		0.96836	2873.26088	-17.61843	-135.47462
Nutrien internal database	AS86-09	Allan	649	44500	27000	1370	2245	510	211			0.93567	475.32766	-17.6	-140
Nutrien internal database	AS86-10	Allan	660	65000	39300	1930	2355	610	323		25.87	0.93239	453.55125	-16.9	-137
Nutrien internal database	ASBR 02-307	Allan	667	62219.22806	38282.51115	2730	2140	767	38.5		39.23	0.94884	3642.33108	-17.61661	-136.96617
Nutrien internal database	RMBR 02-351	Rocanville	670	133343.0157	78929.96882	2840	2910	1240	155.54	4140		0.91283	1932.16276	-6.72953	-71.27641
Nutrien internal database	RMBR 02-350	Rocanville	674	136195.9968	82189.84551	2820	3090	1290	156.79	3750		0.93062	1957.76929	-6.1294	-69.62086
Nutrien internal database	RMBR 02-360	Rocanville	675	133061.458	79230.38216	3790	3250	1200	147.38	3570		0.91824	2034.83527	-7.23455	-75.25013
Nutrien internal database	RS83-02	Rocanville	676	130000	84000	2020	5320	1180	992	4200		0.99645	295.35696	-5.9	-86
Nutrien internal database	ASBR 02-321	Allan	679	61739.12384	36857.79144	2470	1960	496	36.86263	5820		0.92063	3774.76295	-18.14396	-140.03684
Nutrien internal database	RMBR 02-359	Rocanville	701	131986.8612	77271.03499	2540	3620	1480	163.27			0.90283	1821.9642	-6.9653	-72.81993
Nutrien internal database	ASBR 02-306	Allan	702	63815.65522	38492.79331	2960	2210	660	40.71179	4710		0.93019	3532.8289	-18.03944	-140.28065
Nutrien internal database	AS86-11	Allan	704		46600	2280	2770	650	318	5670				-18	-138
Nutrien internal database	RS83-03	Rocanville	704	144900	102000	2280	4170	1870	750	3270		1.08555	435.43432	-6.6	-84
Nutrien internal database	RS86-19	Rocanville	707	136000	130000	1760	3840	2260	880			1.47409	348.31467	-5.5	-80
Nutrien internal database	RS86-20	Rocanville	707	142400	72100	2800	4080	810	720		50.81	0.78081	445.75172	-6.4	-74
Nutrien internal database	ASBR 02-305	Allan	714	47510.30967	24280.30526	580	1830	763	112			0.78811	956.06048	-14.53511	-122.55643
Nutrien internal database	RMBR 02-349	Rocanville	720	140645.5583	77243.10828	2290	6310	929	184.8			0.84694	1715.29801	-2.93483	-58.56617
Nutrien internal database	RS86-21	Rocanville	720	157000	99000	840	7940	1980	1121	1698		0.97242	315.65274	-1.9	-74
Nutrien internal database	CSBR 02-339	Cory	728	153324.5432	51474.16878	2340	26800	8410	995	5190		0.51772	347.29948	-6.02204	-93.19599
Nutrien internal database	ASBR 02-304	Allan	739	139802.3225	56956.21216	1740	18500	5640	696	1104		0.62827	452.71061	-10.62493	-103.04841
Nutrien internal database	AS86-12	Allan	748	180000	120000	1740	5109	20601	812	756		1.02808	499.61102	-14.9	-124
Nutrien internal database	CS92-03	Corv	752	103260	23039	1180	14465	4461	245	519		0.34407	949.90805	-9.7	-102
Nutrien internal database	CS92-04	Cory	757	98170	21919	820	14709	4889	204.5		291.64	0.34432	1081.9346	-15.8	-110
Nutrien internal database	CSBR 02-332	Cory	761	110997.6906	34889.95872	1470	20100	6370	691		327.03	0.48474	362.03572	-10.11333	-99.77738
Nutrien internal database	AS86-13	Allan	765	136000	73000	2410	2370	2400	1174		110.26	0.82776	261.08766	-10.4	-105
Nutrien internal database	ASBR 02-322	Allan	766	184797.2123	107056.0467	2040	6560	2290	359		343.39	0.89338	1160.15628	-14.85646	-123.25398
Nutrien internal database	CS86-16	Corv	770	96400	36000	710	22180	6600	906	1122		0.5759	239.80839	-9.6	-120
Nutrien internal database	ASBR 02-323	Allan	770	192092.2462	111131.5907	2300	6260	2130	337	1149		0.89217	1284.68148	-15.21926	-124.78261
Nutrien internal database	ASBR 02-324	Allan	773	190768.8316	111666.6839	2360	6510	2160	348	1089		0.90268	1235.50272	-14.63325	-123.59319
Nutrien internal database	AS02-03	Allan	776	201924	118552	2530	6867	2169		1080		0.9054		-15	-125.3
Nutrien internal database	AS86-14	Allan	782	196000	173000	1810	8160	2810	2028	843		1.36116	217.82296	-15.1	-125
Nutrien internal database	CSBR 02-338	Cory	784	140536.9388	53623.5709	2280	22000	5980	803			0.58841	394.44865	-11.62683	-107.05793
Nutrien internal database	CS86-17	Corv	787	160000	103500	2220	21740	5650	1720	828		0.99756	209.65589	-8.3	-106
Nutrien internal database	CS92-05	Corv	793	131870	32227	1920	15472	3904	332.7		387.47	0.37687	893.32345	-11.8	-113
Nutrien internal database	CSBR 02-337	Cory	797	183310.8622	86259.60413	3170	19900	3980	873		314.09	0.72567	473.24876	-10.07089	-98.6366
Nutrien internal database	CS92-06	Corv	798	157060	43280	1440	11601	2382	293.9	606		0.42495	1204.42992	-10.4	-103
Nutrien internal database	RMBR 02-358	Rocanville	798	187091.8662	111344.5488	3640	4590	1710	266.73			0.91777	1580.87879	-2.34862	-46.32605
Nutrien internal database	RMBR 02-348	Rocanville	798	190708.8135	113057.402	3770	4570	1630	259.11	1335		0.91421	1658.83091	-2.42213	-45.14805
Nutrien internal database	RS86-22	Rocanville	798	186000	118000	2890	6550	1590	2114	1326		0.97833	198.30035	-2.1	-68
Nutrien internal database	CSBR 02-333	Cory	802	167620.0767	75078.3681	2820	19300	4200	754		203.4	0.69073	501.03749	-11.41984	-104.98676
Nutrien internal database	RMBR 02-357	Rocanville	804	186902.1136	111552.9354	3760	4760	1720	261.32			0.92042	1611.97051	-2.86737	-50.43479
Nutrien internal database	RS86-23	Rocanville	804	227000	135000	2810	7840	1920	2157	1446		0.91712	237.1872	-1.4	-60
Nutrien internal database	RS86-24	Rocanville	804	201500	108000	3930	5410	1050	1190		74.37	0.82655	381.63098	-1.9	-49
Nutrien internal database	RS86-25	Rocanville	807	200600	150000	4300	5540	2490	2000		45.84	1.15313	226.05622	-1.9	-66
Nutrien internal database	RS86-26	Rocanville	809	199000	143000	2160	7620	2000	2200		40.42	1.10816	203.86653	-1.4	-59
Nutrien internal database	CS86-18	Cory	809	171000	81000	1890	25300	4750	2157	654		0.73048	178.67406	-10.8	-112
Nutrien internal database	ASBR 02-303	Allan	817	195319.2916	109578.8707	3240	8790	2790	422			0.86517	1043.1535	-14.38417	-125.96663
Nutrien internal database	CS86-19	Cory	818	199000	130000	2290	22640	1500	2804			1.00742	159.95234	-9.6	-107
Nutrien internal database	CS86-20	Corv	818	194000	173000	1510	18950	4770	2804		371	1.37519	155.93344	-9.9	-107
Nutrien internal database	CS92-07	Corv	825	203150	22565	9870	27846	7380	1366			0.17129	335.18275	-8.4	-100
Nutrien internal database	CS86-21	Cory	831								657.42			-11.6	-108
Nutrien internal database	CSBR 02-334	Cory	837	207984.254	52233.09181	9250	43700	12500	2390			0.38729	196.13183	-7.43246	-94.00327
Nutrien internal database	CS86-22	Cory	845	228000	60000	6300	68500	18300	5956	30		0.40582	86.27713	-8.4	-94
Nutrien internal database	CS86-23	Corv	845	207000	51000	7100	50720	3700	2206			0.37994	211.48539	-9.2	-102
Nutrien internal database	ASBR 02-302	Allan	858	296601.6076	9844.15718	9600	118000	17900	5050	897		0.05118	132.37246	-0.54512	-47.03692
Nutrien internal database	ASBR 02-301	Allan	865	348724.7538	4598.09848				6520	201		0.02033	120.54542	-3.889	-105.68146
Nutrien internal database	CS86-24	Cory	887	355000	54870	16300	18200	28400	2174			0.23836	368.03095	-3.6	-67
Nutrien internal database	CSBR 02-336	Cory	901	310759.7435	6985.86547	20100	124000	20100	5400		3284.02	0.03467	129.70196	1.79291	-53.22946
Nutrien internal database	CSBR 02-335	Cory	905	318746.0311	6947.023	19200	124000	20200	5490	258		0.03361	130.85429	0.64201	-48.34283
Nutrien internal database	CS86-25	Corv	915			13090				273				-1.26	-65
Wittrup and Kvser (1990)	11	Corv	55	709	1520	166	30	7	9			3.3061	177.54942	-18.8	-150
Wittrup and Kvser (1990)	41	Allan	111	354	2050	3	73	6	32			8.93036	24.93267	-17.5	-129
Wittrup and Kvser (1990)	42	Allan	144	530	2280	6	85	8	32			6.63403	37.32858	-17.4	-136
Wittrup and Kvser (1990)	43	Allan	310	1020	6250	45	362	84	76			9.44927	30.24838	-13.4	-119

Wittrup and Kvser (1990)	12	Corv	539	35600	28000	1360	1964	870	196	1.2129	409.36382	-13.5	-115
Wittrup and Kvser (1990)	117	Cory	569	29200	17000	430	1954	820	155	0.89781	424.58699	-16.8	-143
Wittrup and Kvser (1990)	18	Corv	570	29600	17000	430	2202	670	12900	0.88568	5.17151	-16	-127
Wittrup and Kvser (1990)	119	Cory	588	96400	36000	710	22180	6600	906	0.5759	239.80839	-9.6	-120
Wittrup and Kvser (1990)	145	Corv	603									-16.8	-136
Wittrup and Kvser (1990)	118	Cory	612	24900	18000	540	2010	830	168	1.11479	334.04548	-17	-134
Wittrup and Kvser (1990)	411	Allan	621	33800	24200	1240	2098	530	207	1.10412	368.01192	-18	-139
Wittrup and Kvser (1990)	412	Allan	637	40900	25700	1390	2059	520	208	0.96901	443.17525	-18.1	-138
Wittrup and Kvser (1990)	45	Allan	643	42700	24900	1250	2007	330	211	0.89927	456.10092	-18.3	-139
Wittrup and Kvser (1990)	46	Allan	648	44500	27000	1370	2245	510	211	0.93567	475.32766	-17.6	-140
Wittrup and Kvser (1990)	413	Allan	660	65900	39300	1930	2355	610	323	0.91966	459.83119	-16.9	-137
Wittrup and Kvser (1990)	47	Allan	704		46600	2280	2770	650	318			-18	-138
Wittrup and Kvser (1990)	414	Allan	748	180000	120000	1740	5109	2060	1810	1.02808	224.13489	-14.9	-124
Wittrup and Kvser (1990)	48	Allan	765	136000	73000	2410	2370	2400	1170	0.82776	261.98026	-10.4	-105
Wittrup and Kvser (1990)	110	Cory	770	101000	42000	940	24500	4800	863	0.64128	263.77043	-11.2	-103
Wittrup and Kvser (1990)	49	Allan	782	196000	173000	1810	8160	2810	2030	1.36116	217.60835	-15.1	-125
Wittrup and Kvser (1990)	14	Corv	787	160000	103500	2220	21740	5650	1720	0.99756	209.65589	-8.3	-106
Wittrup and Kvser (1990)	121	Cory	818	199000	130000	2290	22640	1500	2800	1.00742	160.18084	-9.6	-107
Wittrup and Kvser (1990)	122	Corv	845	228000	60000	6300	68500	18300	5950	0.40582	86.36413	-8.4	-94